Fall 2016

Experimental study on the impact of carbon nanomaterials on coke formation

Matthew James Panzer
University of Iowa

EXPERIMENTAL STUDY ON THE IMPACT OF CARBON NANOMATERIALS ON COKE FORMATION

By

Matthew James Panzer

A thesis submitted in partial fulfillment
of the requirements for the Master of
Science degree in Mechanical Engineering
in the Graduate College of
The University of Iowa

December 2016

Thesis Supervisor: Associate Professor Albert Ratner

Graduate College
The University of Iowa
Iowa City, Iowa

CERTIFICATE OF APPROVAL

_____

MASTER'S THESIS

_____

This is to certify that the Master's thesis of

Matthew James Panzer

has been approved by the Examining Committee
for the thesis requirement for the Master of Science degree
in Mechanical Engineering at the December 2016 graduation.

Thesis Committee: _____
Albert Ratner, Thesis Supervisor

_____
James Buchholz

_____
Shaoping Xiao

ACKNOWLEDGEMENTS

I would like to thank Professor Ratner for all of his generous support and guidance throughout my time as a student. I would also like to thank Mohsen Ghamari and Kayla Denson for helping me setup, organize, and conduct experiments. To all my friends who have put up with my busy schedule, I am thankful to have you in my life. Lastly, I would like to thank my parents for their unwavering support through thick and thin. Without their sacrifices, I would not be where I am today.

ABSTRACT

Thermal management is a major concern of jet engine development. During flight, engine components reach extreme temperatures as a result of frictional heating due to elevated airflow velocities. Jet fuel is used as a coolant to dissipate heat throughout the engine. This cooling process induces temperature and pressure increases within the fuel. At temperatures above 325°F, hydrocarbon fuels start to become thermally unstable, leading to the formation of solid deposits, known as coke. This paper outlines an experimental study that was conducted to further examine the coking mechanism. Specifically, a complete experimental setup and procedure was designed to simulate coke deposit formation in a controlled laboratory environment. Fuel was thermally stressed up to 330°C at 10 Bar for approximately 6 hours. Tests were conducted using plain Jet-A fuel and Jet-A fuel with 0.1% carbon nanoparticle and nanotube additives. Deposit formation on stainless steel samples were analyzed using Scanning Electron Microscopy imaging. Results showed that the introduction of nano-additives into the fuel yielded less deposit formation and build up on stainless steel surfaces. Both nanoparticles (100 nm diameter) and nanotubes (8 – 15 nm diameter, 0.5 – 2 μm length) were found to be effective at suppressing coke deposits above 300°C.

PUBLIC ABSTRACT

Thermal management is a major concern of jet engine development. During flight, engine components reach extreme temperatures as a result of frictional heating due to elevated airflow velocities. In order prevent overheating, jet fuel is used as a coolant to dissipate, or absorb the heat from the engine. As the fuel absorbs the waste heat, the temperature and pressure increases. At temperatures above 325°F, hydrocarbon fuels start to become thermally unstable. Thermal stability is characterized as a fuel's tendency to form solid deposits on fuel lines, nozzles, intake valves, and other engine components. This process is also referred to as coking, and is driven by complex chemical mechanisms that are triggered by increased temperatures.

This paper outlines an experimental study that was conducted to further examine the coking mechanism. Specifically, a complete experimental setup and procedure was designed to simulate coke deposit formation in a controlled laboratory environment. Fuel was thermally stressed up to 330°C at 10 Bar for approximately 6 hours. Tests were conducted using plain Jet-A fuel and Jet-A fuel with 0.1% carbon nanoparticle and nanotube additives. Results showed that the introduction of nano-additives into the fuel yielded less deposit formation and build up on stainless steel surfaces. A reduction in deposit formation would lead to reduced maintenance costs and improved operation for military and commercial jet engines.

TABLE OF CONTENTS

LIST OF TABLES

LIST OF FIGURES

Chapter 1: Introduction

1.1 Thermal Management of Gas Turbines

Thermal management is one of the main issues facing the design and development of gas turbine engines. As engine technology advances, power output, flight velocities, and efficiencies continue to increase. Temperature is among the key parameters affected by increased power and flight speeds. At supersonic and hypersonic flight speeds, inlet air temperatures increase as a result of extreme frictional effects. In order to keep engine components from overheating, alternative cooling systems are required. Jet fuel has traditionally been used as a coolant, or heat sink, in order to dissipate some of the heat generated by the engine during operation. This technique is known as fuel-cooled thermal management [10].

Fuel-cooled systems are preferred compared to other systems because they are more compact and efficient. Systems utilizing air as a heat sink require bulky equipment such as heat exchangers and fans that add unnecessary weight to the aircraft. Hydrocarbon fuels are able to retain large amounts of thermal energy through endothermic reactions, thus making them an effective cooling medium [10]. However, this benefit comes at a price. When hydrocarbon fuels are elevated to high temperatures, thermal instabilities can lead to the formation of solid deposits, or coke.

Due to the complexity of jet fuels, significant research has been conducted on how different fuels react to the extreme environments experienced within jet engines. Specifically, the thermal stability of fuels is a serious concern for engine performance and operation. Thermal stability is defined as a fuel's tendency to form deposits on jet engine components such as fuel lines, nozzles, intake valves, fuel injectors, and combustion chamber surfaces [1]. The formation of solid deposits, known as coking, can have a detrimental effect on engine performance and lead

to elevated maintenance costs. When fuels are heated to supercritical temperatures, typically above 325°F, the formation of solid deposits and coke begins to occur [16]. In gas turbine applications, fuel temperatures consistently reach this set point, and in turn increase the susceptibility to form deposits.

1.2 Project Objective

The objective of this thesis and project was to further examine the coking mechanism that occurs among jet fuels. Specifically, an experimental setup capable of simulating coke formation and deposition on stainless steel surfaces was designed. Jet-A fuel temperatures and pressures similar to real engine conditions were simulated in a controlled laboratory environment. After achieving valid coking results, different nanomaterials were added to the Jet-A fuel to examine the effects on deposit formation and build up on stainless steel. Specifically, Carbon Nanoparticles and Multi-Walled Nanotubes were utilized as fuel additives and tests were conducted under same conditions as the preliminary Jet-A tests. Scanning electron microscopy (SEM) images were used to compare the deposit formation between the different fuel types. A complete analysis was conducted detailing the effects that nanomaterial fuel additives could potentially have on coke deposit formation.

Chapter 2: Background and Literature Review

2.1 Jet Fuel Overview

Thermal instabilities are most prevalent in hydrocarbon based fuels which are used in jet engines. Early jet engines utilized kerosene as the fuel source due to availability. Compared to gasoline, kerosene was readily available. Following World War II, “wide-cut” fuel was introduced by the Air Force as a mixture of kerosene and gasoline [3]. The motivation behind this fuel was also based on availability. It was thought that large quantities of only gasoline or only kerosene would be difficult to obtain, thus, a mixture of the two was utilized and known as JP-4. However, wide-cut fuels were found to not be optimal due to their high volatility and evaporation that occurred at high altitudes [3].

During the 1970s, the Air Force began utilizing kerosene based fuels again such as JP-8. Today, JP-8 remains the main fuel used by the Air Force [3]. It is a kerosene based fuel consisting of Jet-A and additives to enhance performance. Jet-A and Jet-A1 are the main fuels used commercially throughout the world. The main difference between commercial and military fuels is the amount of additives. Military fuels contain additional additives such as antioxidants, metal deactivators, and thermal stability additives. Commercial fuels such as Jet-A, may only have an antioxidant, if any additives. For testing purposes, the use of Jet-A should yield greater coke deposits due to the lesser amount of coke fighting agents.

Prior to designing an experiment capable of simulating coke formation, research was conducted on the conditions jet fuel experiences during engine operation. Temperature and pressure will vary based on the loading of the engine. For example, during takeoff and acceleration, temperatures and pressures will be much greater than during normal flight or descent conditions. Table 2.1 outlines the fuel temperatures, pressures, and residence times experienced throughout various engine components during flight idle conditions according to Hazlett [8]. These conditions are of interest because they represent the conditions that an engine will experience for the greatest duration. While takeoff conditions will be greater, the duration will also be much shorter.

Table 2.1: Fuel parameters at flight idle conditions [8].

Fuel System Component	Single Pass Residence Time, s	Fuel Temperature, °F (°C)	Pressure, psia	Surface Temperature, °F (°C)
Fuel tank	5×10^3-5×10^3	-40-120 (-40-49)	2.5-3.5	-50-130(-46-54)
Tank boost pump	15-30	123-128 (51-53)	25-35	Fuel
Engine first stage pump	13-32	127-150 (53-56)	75-100	Fuel
Engine oil cooler	0.7-1.4	245-320 (118-160)	75-400	200-320 (93-160)
Engine gear pump	0.5-0.6	245-320 (118-160)	350-400	Fuel
Fuel filter	0.5-1.0	245-320 (118-160)	75-400	Fuel
Main engine control	1.1-5.0	245-320 (118-160)	350-400	Fuel
Cruise servos	1.0-20	245-320 (118-160)	350-400	Fuel
Bypass recirculation	-	245-320 (118-160)	75-100	Fuel
Generator oil cooler	10-15	245-320 (118-160)	40-100	320 (160)
Fuel nozzles	0.15-0.8	300-400 (150-200)	40-100	450-500 (232-288)

During heavy engine operation (Ma>3), fuel temperatures and pressures may reach as high as 800 K and 300 psi, with short residence times [17]. Since these conditions would be very difficult to simulate in a controlled laboratory setting, lower temperatures and pressures, with longer residence times, present a more appealing option for an experimental setup and procedure.

2.2 Thermal Stability of Fuels

As introduced previously, thermal stability is defined as a fuels tendency to produce solid particulates, also known as coking. Temperature is one of the key contributors to initiating the reactions that lead to coke formation. The mechanisms that dominate fuel decomposition are temperature dependent, and thus as the temperature increases, the coking mechanisms change as well. The two most widely studied mechanisms are autoxidation and pyrolysis. Autoxidation occurs at temperatures between 290 – 400°C while pyrolysis occurs at fuel temperatures exceeding 400°C [7]. Both mechanisms are characterized as free radical reactions. However, at lower temperatures, autoxidation is driven by an oxidation reaction of radicles that leads to the formation of solid particulates [7]. On the contrary, pyrolysis is characterized by cracking reactions that lead to the formation of larger (in molecular weight) compounds as the byproduct [16].

Although different in the kinetics, both mechanism follow the same general method for particle deposit within real engine applications. Figure 2.1 outlines a general coking process demonstrating deposit build up on a surface. Given the appropriate temperature, coking reactions will initiate within the fuel. Via mass transfer, solid particulates transfer from the bulk liquid to a surface. Closer to the surface, within the boundary layer, increased turbulence subsequently increases the mass transport rate [5]. In addition, Kendall and Mills discovered that metal surfaces, such as stainless steel, could act as a catalyst and provoke oxidation reactions leading to greater deposits [11]. When tested among other metal surfaces (e.g. aluminum, copper, etc.) stainless steel was found to yield greater coke deposits; possibly indicating a more favorable chemical composition for deposits to bond too.

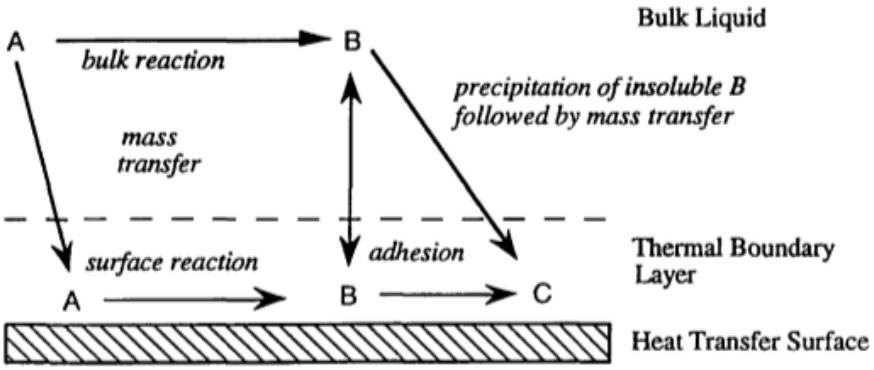

Figure 2.1: General coking mechanism [18].

2.2.1 Autoxidation Mechanism

The effects of temperature on the autoxidation of fuels is very complex and not fully understood. In general, when oxygen rich fuel (~70 ppm) reaches above 350°F, the oxygen begins to react and form free radical species which initiate other oxidation reactions to occur [16]. This process is what leads to deposit formation and build up. Balster and Jones concluded that during the autoxidation regime, the formation of coke deposits occurs during oxygen depletion, and as fuel temperature increases, so does the oxygen depletion rate [4]. However, after completing tests at temperatures of 185°C and 225°C, an inverse relationship between temperature and deposition rate was found. Greater deposition rate was found to occur when the fuels (Jet-A, JP-5, and JP-8) were heated to 185°C. It was concluded that temperature does not have a large effect on the formation of deposits for fuels that are thermally stable [4]. Instead, fuels that oxidize more easily, are more thermally stable and less likely to form deposits [9]. The following reactions outline the autoxidation kinetic scheme that better underscores the reasoning behind the inverse temperature relationship, as reported by Watkinson and Wilson [18].

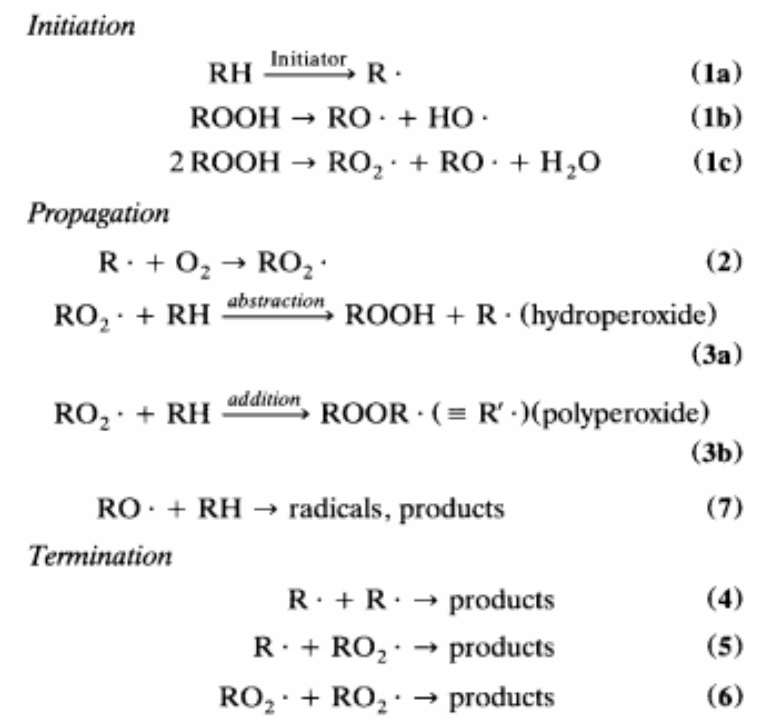

Figure 2.2: Autoxidation mechanism [18].

Figure 2.2 outlines the reactions that make up the autoxidation mechanism. Thermal decomposition of the hydrocarbon RH leads to the formation of the radical R· in initiation step (1a). With ample oxygen levels within the fuel, the radical R· oxidizes into radical RO_2· in step (2). Propagation continues to occur through steps (3a) and (3b) and forms hydroperoxides and polyperoxides. The hydroperoxides (ROOH) are what Balster and Jones pinpointed as the contributors to the inverse temperature dependence findings. Thermally unstable fuels were found to contain impurities such as sulfur and other metals that reacted with ROOH and ROOR peroxides [4]. These additional reactions slowed oxidation, and hence, led to greater deposit formation. Thermally stable fuels were found to not have as many impurities, and thus the fuels oxidized easier with less reactions and less deposit formation.

2.2.2 Pyrolysis Mechanism

The pyrolysis mechanism typically becomes the dominant route to solid deposit formation when fuel temperature exceeds 400°C. Deposits form within this regime as a results of thermally unstable long-chain alkanes [2]. At greater temperatures, chemical bonds are broken and large alkanes are converted into smaller alkanes and hydrogen. This mechanism is driven by thermal and catalytic cracking reactions and polymerization [16]. These reactions typically result in the formation of solid compounds with greater molecular weights than the compounds formed via the autoxidation mechanism [7]. Figure 2.3 below underscores the temperature dependence of the different mechanisms.

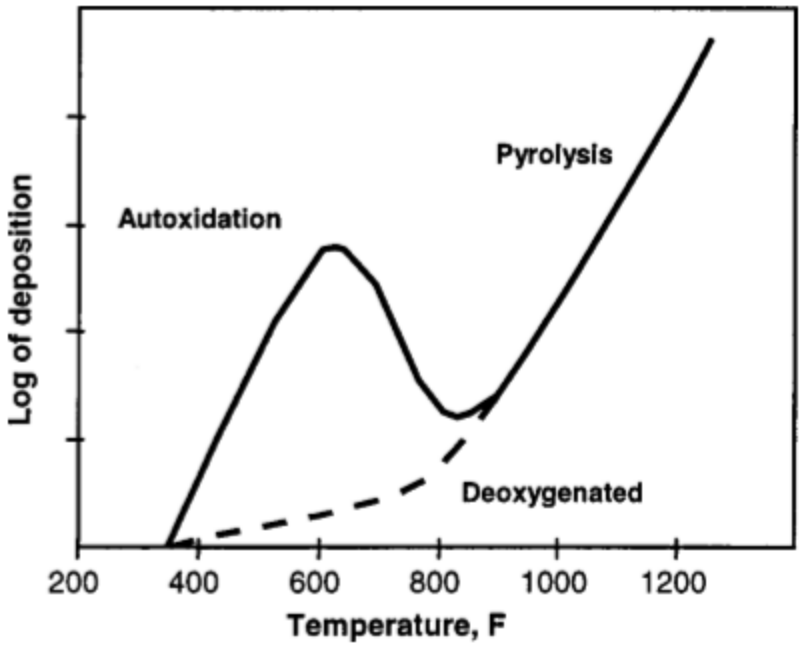

Figure 2.3: Deposition rates for jet fuel with respect to temperature under different mechanisms [16].

2.3 Factors Affecting Coking

One of the main contributing factors to coking and deposit formation is the amount of dissolved oxygen in the fuel. Due the nature of the autoxidation mechanism, in fuels with low levels of dissolved oxygen (~1 ppm), the oxidation process will not occur. Figure 2.3 highlights this point between deposition rate and temperature. Note the difference in deposition between the autoxidation and deoxygenated plots. Autoxidation is driven by the fuels relative oxygen content, and thus research has been conducted on reducing the oxygen content in fuels to eliminate or reduce coking. In a study conducted by Spadaccini and Huang in 2002, deoxygenated fuels were tested against oxygen saturated fuels. Deoxygenated fuel was created by running air saturated fuel through a membrane deoxygenator, which essentially was a shell and tube heat exchanger. The shells in this heat exchanger were coated with a thin membrane layer, which would invoke oxygen diffusion. This system resulted in dissolved oxygen forming on the surface of the shells as the fuel was pumped through. Both normally saturated fuel (~70 ppm) and deoxygenated fuels (~1 ppm) were heated above 600°F. Results revealed that the deoxygenated fuel led to significantly less coke formation than the normally saturated Jet-A and JP-8 fuels, seen below in figure 2.4 [15]. At a wall temperature of 635°F, the coke formation was almost eliminated for each of the deoxygenated fuels. It may be noted that JP-8+100 experienced the least amount of surface deposition. JP-8+100 is a military fuel that contains additional additives to improve thermal stability and reduce deposit formation.

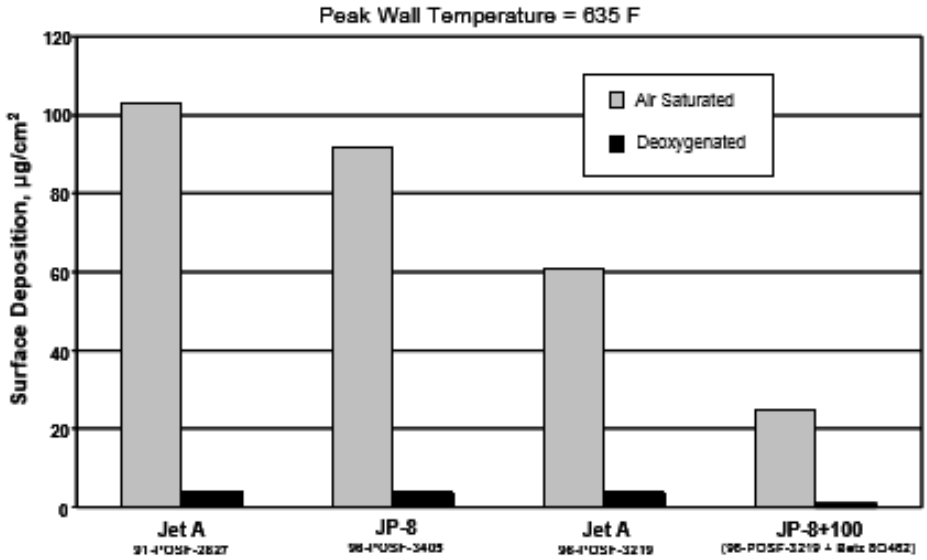

Figure 2.4: Coke deposit formation between air saturated and deoxygenated fuels [15].

In addition to the relative oxygen content in the fuel, temperature plays an enormous role in the coke formation. As stated previously, the two main mechanisms (autoxidation and pyrolysis) are temperature dependent. The autoxidation regime operates between 290 – 400°C while pyrolysis operates above 400°C [7]. Initial propagation of the chemical kinetics behind deposit formation is driven by temperature. Without increased fuel temperatures, coking reactions will not initiate and propagate, making it the most important factor in fuel degradation. Another contributing factor that was investigated was pressure. In a study conducted by Spadaccini and Huang, the effects of temperature and pressure on deposit formation were analyzed. Tests were run under low and high pressures with the same temperatures. Results indicated that increased pressure only has a small impact on deposit formation under the autoxidation mechanism [16]. Specifically, increased pressure leads to increases in viscosity and density of the fuel, which should only have a small impact on mass transfer at lower

temperatures. However, at greater temperatures in the pyrolysis mechanism, increased pressure will lead to increased residence times and chain breaking reactions may be accelerated [16]. In short, pressure has been found to not be a significant factor in deposit formation under the autoxidation regime, but should increase fuel degradation under the pyrolysis regime.

2.4 Fuel Additives

As discussed in section 2.1, the main difference between commercial and military fuels is the amount of additives military fuels contain compared to commercial fuels. The goal of fuel additives is to increase the thermal stability of the fuel in hopes to reduce or eliminate deposit formation. One additive of interest is the thermal stability additive +100, which is added to JP-8 fuel to form JP-8+100. This chemical additive is particularly unique as it does not directly affect the chemistry of the fuel, but rather reduces deposit formation on wetted metal surfaces [14]. Essentially, instead of altering the chemical kinetics responsible for coking, the additive simply works to reduce deposit build up to engine components such as fuel lines, nozzles, heat exchangers, etc.

In a study conducted at the Aeronautical and Maritime Research Laboratory, the effect of the +100 additive was examined verses additive-free fuels. All fuels were stressed at 250°C, 350°C, and 400°C within the same testing apparatus. Results revealed that the fuels with the +100 additive led to significantly less carbon deposition on sample surfaces at 250°C and 350°C. While at 400°C, the opposite occurred and there was actually an increase in deposit build up for the +100 additive case [14]. These findings proved that under low temperatures within the autoxidation mechanism, the +100 additive can be used to significantly reduce coke deposit build up. However, this additive has a thermal limit between 350°C and 400°C where the additive is

no longer an effective solution for reducing deposit build up. Although the +100 additive fails at temperatures greater than 400°C, the addition of the additive to fuels does in fact increase the thermal stability of the fuel. Additive-free fuels demonstrated much greater coking rates at the 250°C and 350°C temperatures. Hence, the +100 additive raised the minimum temperature required to initiate the formation of solid deposits on metallic surfaces.

2.5 Previous Coking Experimental Setups

Even though there is still much to study about the chemical kinetics that govern coking, there has been sufficient research conducted on simulating coke deposit formation and fuel degradation. In this section, different experimental setups and procedures were analyzed in order to determine optimal setups to simulate coke formation. The first experimental setup analyzed was designed by Spadaccini and Huang for their study on deposit formation and mitigation. The setup used for their tests can be seen below in figure 2.5 [16]. This rig consisted of five separate flow paths where different configurations, pipe geometries, or conditions could be simulated. The testing procedure consisted of pumping fuel into the fuel accumulator section, where it was pre-pressurized using nitrogen. Fuel was then pre-heated up to 350°F before being pumped into the test section, where the fuel was heated to temperatures ranging from 350 – 1000°F. Finally, the fuel was cooled and pumped into a collector waste reservoir. Deposits were analyzed by removing the heat exchanger tubes the fuel was pumped through in the test section. Tubes were then cut down into smaller samples, rinsed in hexane, and then analyzed using a Carbon Determinator to quantify the carbon deposits formed. Testing showed the greatest amount of deposits formed with a fuel temperature of 600°F (315°C).

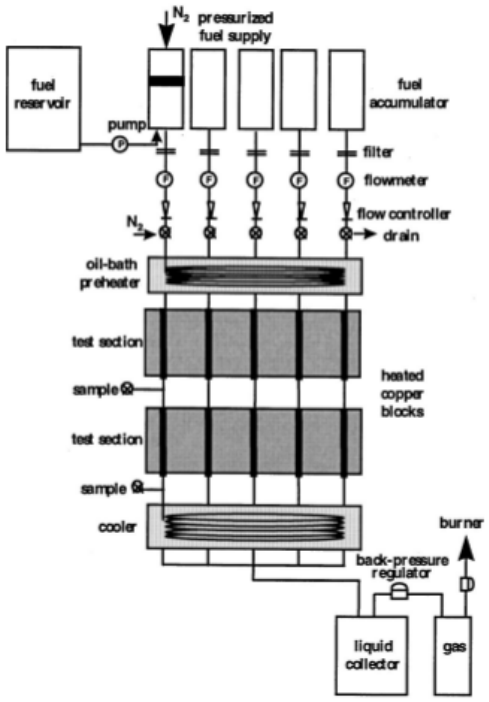

Figure 2.5: Testing apparatus used by Spadaccini and Huang [16].

Gul, Rudnick, and Schobert designed an experimental setup to study the effect of reaction temperature on deposit formation at Pennsylvania State University [7]. Their setup can be seen in detail in figure 2.6. Their testing methodology was more simple than Spadaccini and Huang's setup. The procedure simply consisted of pumping fuel from a pre-heated reservoir to a heated chamber, where the fuel would be thermally stressed. After which, the fuel was pumped into a waste reservoir to cool. The goal of this research was to simulate coking via the pyrolysis mechanism, and thus greater temperatures of 470 – 490°C were simulated.

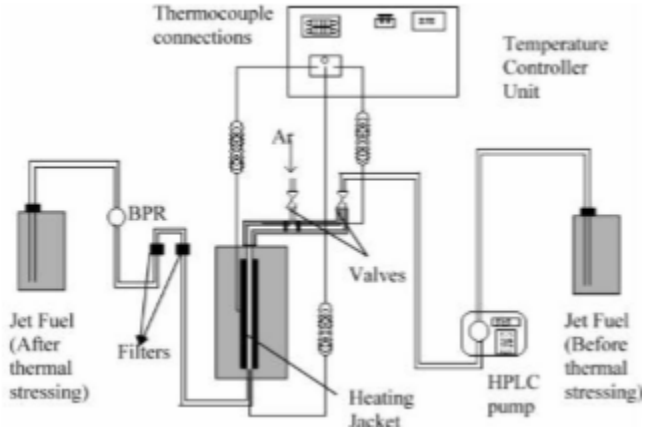

Figure 2.6: Testing apparatus used by Gul, Rudnick, and Schobert [7].

The final experimental setup analyzed was designed at the University of Dayton to study surface effects on deposits from jet fuels [5]. This setup is displayed in figure 2.7 and followed a very similar design and procedure as described in figure 2.6. Fuel was pumped from a pre-heated reservoir into two heating blocks. Bulk fuel temperatures were recorded up to 230°C prior to being pumped out of the heating section and to the sump. Similar to Spadaccini and Huang's procedure, at the conclusion of a test, fuel tubes were removed, rinsed in hexane, and then cut into 50 mm samples. The samples were analyzed using a carbon analyzer, as well as scanning electron microcopy (SEM) images.

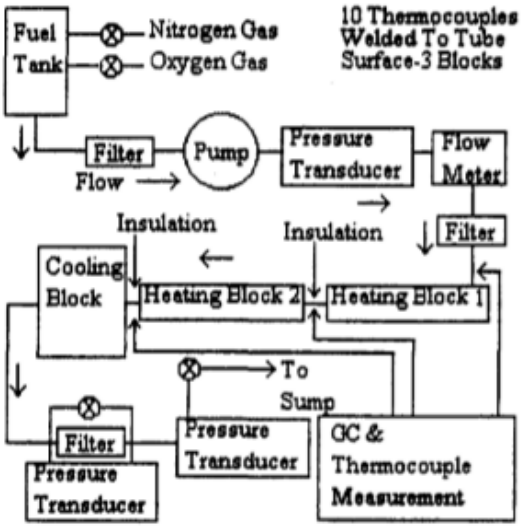

Figure 2.7: Testing apparatus used by University of Dayton [5].

Chapter 3: Experimental Setup

3.1 Experimental Overview

As stated previously, the goal of this project was to determine the effects carbon nanomaterials have on fuel coking and deposit build up. In order to examine the effects, an experimental setup capable of simulating jet fuel coking needed to first be developed. Past research conducted on coke formation and solid deposit build up utilized pressure and temperature based experiments as described in section 2.5. In general, these tests pumped fuel through a heating block, where fuel temperature increased until deposits began to form.

The testing methodology used in this project followed the same concepts as previous successful experiments. A single testing chamber was used where the fuel would be heated and pressurize. The fuel was left at a constant pressure and maintained within a temperature range for the duration of the test. Due to evaporation losses, fuel would have to be periodically added every hour or so in order to conduct multiple hour long tests. Further descriptions of the testing procedure will be described in the following sections.

3.2 Testing Parameters

Based off the past experiments conducted by the United Technologies Research Center and the data presented in figures 2.3 and 2.4, fuel temperatures of approximately 315 – 330°C typically lead to large deposition rates within the autoxidation regime [16]. With temperature being the key contributor to initiating autoxidation reactions within the fuel, extreme pressures (100 Bar) were found to be unnecessary to achieve coking. Instead, a lower pressure range of about 10 Bar (150 psi) was to be used to pressurize the fuel system. The final testing parameter

was test duration. In general, the longer the fuel is stressed, the greater coke deposit build up. Testing times of five to six hours were selected as this would give ample time for fuel degradation and deposit formation. In addition, this time frame allowed for one experimenter to conduct a test. Jet-A was selected as the fuel choice based off of its similarities to commercial and military fuels, as well as its availability from the Iowa City Municipal Airport.

3.3 Design of Experimental Apparatus

Development of the testing rig consisted of designing a system capable of reaching all of the testing parameters described in the previous section. Most importantly, fuel temperatures of 315 – 330°C needed to be reached and maintained for the duration of the test. A constant wattage heat cable and a thermocouple – based temperature control system was utilized to heat and maintain the testing chamber. Nitrogen was used as the pressurizing agent. Two fuel reservoirs were used in conjunction with the testing chamber. One fuel tank, located above the testing chamber housed preheated fuel. The second tank, located below the testing chamber housed the waste fuel. A full testing schematic can be seen in figure 3.1.

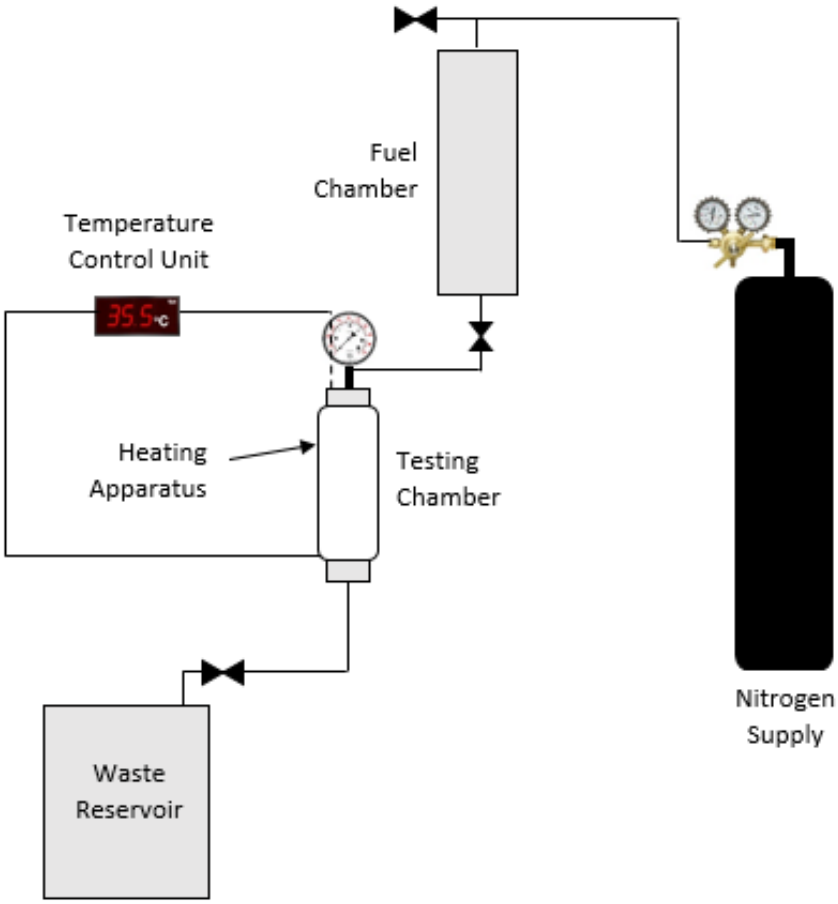

Figure 3.1: Experimental schematic.

3.3.1 Testing Chamber and Fuel Reservoirs

The testing chamber used was a simple stainless steel cylinder seen in Figure 3.2. The chamber had an internal volume of 700 mL, and a height of 14.25 inches and diameter of 2.25 inches. The wall thickness was 0.25 inches. The chamber had two ports drilled into the top section and one port at the bottom, each of which were ¼ NPT pipe thread connections. The top section could be unscrewed and taken off to access the inside of the chamber. The bottom section was chemically bonded using JB Weld in order to ensure a tight seal.

Figure 3.2: Testing chamber without heating apparatus.

A four-way connector was attached to one of top ports. This connector housed a pressure gage, relief valve, and the fuel inlet line. The pressure gage provided the fuel pressure inside of the chamber. The relief valve was a pop safety valve set to release if the pressure exceeded 225 psi. The fuel inlet line was fed from the pre-heated fuel tank, which housed preheated Jet-A fuel. The second port on the top is where the thermocouple was installed. The thermocouple used was an Omega K-type, 1/8-inch diameter and 15 inches long. The fuel exit line was connected at the bottom port. This line fed into the fuel waste reservoir, filled with the post-heated Jet-A fuel.

The preheated fuel chamber was located above the testing chamber seen in Figure 3.3. This pressure vessel was used to hold excess fuel prior to being added to the testing chamber, where it would undergo heating. A three-way connector was installed at the top of the vessel. A pressure relief valve was connected to one of the ports. A nitrogen pressure line was connected to the other port. This ¼-inch plastic line was connected the lab nitrogen tank. At the bottom of the vessel was a single fuel line that was fed into the testing chamber. This line was ¼-inch copper due to the greater temperatures it would experience being closer to the testing chamber. A high temperature ball valve was used on this line that allowed the nitrogen to be cut off. Subsequently, this would stop the pressure supply into the testing chamber.

The waste reservoir was placed below the testing chamber seen in figure 3.4. This three-gallon tank allowed for waste fuel to be emptied out of the testing chamber. The waste fuel line attached at the bottom of the testing chamber fed directly into the reservoir, which was kept at atmospheric pressure. This line was also utilized ¼-inch copper tubing as the waste fuel leaving the testing chamber would be over 300°C. A high-temperature ball valve was attached at the end of the line. When opened, fuel would evacuate out of the testing chamber and fill into the waste reservoir due to the pressure difference between the two vessels.

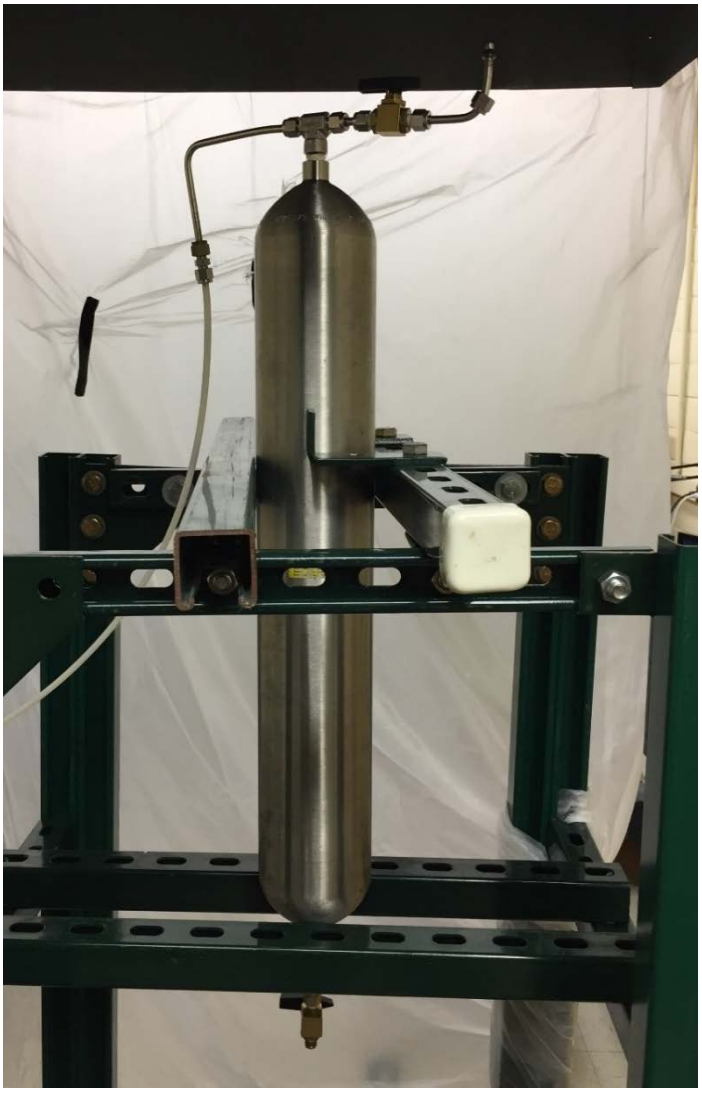

Figure 3.3: Pre-heated fuel vessel.

Figure 3.4: Waste fuel reservoir.

3.3.2 Heating and Pressure Apparatus

In order to reach fuel temperatures above 300°C, a significant amount of heat generation was required. Initial techniques proposed were to pump superheated nitrogen through copper tubing around the testing chamber. This technique would not only be difficult to implement, but would be costly. Past experimenters in the lab utilized electric heat cables that could be wrapped around the chamber and oriented in any position. Results proved the cable to be very effective at obtaining fuel temperatures above 300°C. Thus, the final heating technique selected was a 312 Watt electrical heating cable. The cable was made of fiberglass yarn and was 4 feet long, ½ inch wide, and 1/8 inch thick. A 120VAC power cord with a two-prong plug was attached to the end of the cable. Once plugged in, the cable immediately begins to heat up, providing 312 Watts of heat generation. The cable that was used for all tests can be seen in figure 3.5.

Figure 3.5: 313 Watt heat cable with 120VAC plug.

Internal fuel temperature was monitored using an Omega K-type thermocouple attached at the top of the testing chamber. This thermocouple was positioned to record the temperature at the center of the chamber. The output was attached to a temperature controller module that gave the real-time temperature output. The heating cable was also attached to the same module, which allowed for specific temperature to be selected and held. While the temperature was below the set point, the module supplied continuous power to the heat cable. Once the temperature exceeded the set point, the power supply would be cut off. Therefore, the module allowed for temperature control throughout the duration of the test. Figure 3.6 below shows the temperature control module with a live temperature reading.

Figure 3.6: Temperature control module.

Nitrogen was used as the pressurizing agent for all tests. Supply came from an industrial Pentair tank. Pressure levels were controlled via the regulator attached at the outlet of the tank. From the regulator, the pressure was fed into the pre-heated fuel reservoir, located above the testing chamber. This reservoir was connected directly to the testing chamber. The pressure inside of the testing chamber was monitored from the pressure gage attached at the top of the chamber.

Chapter 4: Experimental Procedure

4.1 Setup Procedure

Setup for each test required checking and assembling all of the components and systems discussed in Chapter 3. Prior to testing, stainless steel samples to capture the coke deposits were machined out from a 0.5-inch diameter stainless steel rod. Each sample was cut 0.25 inches thick and can be seen in figure 4.1 below. The goal of using these samples was to allow coke deposits to form on the surface. The reason for the small size was to ensure that the samples would be able to fit inside the SEM microscope, which had a limited sample size range. Specifically, specimen sizes were required to be less than 1-inch-long and 0.5 inches tall. Hence, samples were cut prior to testing to comply with SEM requirements.

Figure 4.1: Plain stainless steel sample to be used in experiments.

The first step in the assembly procedure was to remove the top section of the testing chamber and insert stainless steel samples for the given test. The top section could then be screwed back on, and tightened using a vice grip and wrench to ensure a tight fit. Also to note,

all connections were wrapped with Teflon tape. After the samples were inserted and the testing chamber was sealed, the electric heating cable was attached. This consisted of wrapping and

connecting the electric heat cable around the chamber seen in figure 4.2. The four-foot-long cable was wrapped around the chamber with about an inch of separation between each pass. This was done in order to disperse the heat load evenly throughout the entire chamber. The cable was tied off at both ends, and tapped down with heat-resistant tape. Lastly, in order to reduce convective heat loss, the entire chamber was insulated with a layer of Superwool fiber and aluminum foil, better seen in figure 4.3.

Figure 4.2: Testing chamber with heat cable installed.

With the testing chamber assembled, it was then placed in the testing stand and attached to the pre-heated fuel reservoir and the waste vessel. Figure 4.3 shows the fully insulated testing chamber installed in the testing stand and connected to each vessel. As stated in Chapter 3 connections between the vessels were all ¼-inch copper tubes. The copper tube connecting the pre-fuel reservoir with the testing chamber was coiled in order to increase the length of the tube. This was done to prevent heated fuel from expanding back into the pre-heated reservoir. During testing, the fuel will undergo a small thermal expansion and induce expansion back up into the pre-heated tank. By increasing the fuel line length, this created a larger volume for the fuel to

expand back into, which prevented already heated fuel from expanding back into the pre-heated reservoir.

Figure 4.3: Fully insulated testing chamber connected to the pre-heated vessel and waste reservoir.

The last step was to add the fuel to the system. Each test began with about 1000 mL of fuel. This was enough to completely fill the testing chamber and have about 300 mL left in the pre-heated reservoir above. Fuel was added to the top reservoir and then emptied into the testing chamber. In order to completely fill the chamber, the thermocouple had to be removed to allow air to escape from the chamber as the fuel was added. Once completely filled, the thermocouple was reattached and all connections were checked and re-tightened. At this point, the system was ready for pressurization and heating to commence.

4.1.1 Addition of Nanomaterial to Fuel

The procedure described in section 4.1 applies to all tests, however, for tests involving nano-additives, additional steps were required to adequately mix the fuel. One of the main concerns with using nano-additives was to ensure that the particles would remain evenly dispersed throughout the fuel during testing. If not properly mixed, the particles tend to coagulate, or clot together. This can lead to large clusters and subsequently non-uniform fuel compositions.

Tests utilized two different types of nanomaterials. Carbon Nanoparticles (CNP) and Multi-Walled Carbon Nanotubes (MWNT). CNPs had average diameters of 100 nm, while MWNTs had outer diameters of 8 – 15 nm and lengths of 0.5 – 2 μm. Based off of the nanoparticle research conducted by Mohsen Ghamari, CNP and MWNT weight percentages of 0.1% paired with 1.5% Span 80, nonionic surfactant was found to yield stable homogenous mixtures [6]. Surfactant reduces the surface tension between substances, and proves to be beneficial in reducing particle clotting. Differences arise between the mixing techniques required for the two types of nanomaterials. Both fuel-particle combinations were mixed using a 300W Ultrasonic Homogenizer (Biologics 3000MP), seen in figure 4.4. For CNPs, the mixing process was programmed per the settings in table 4.1. On/off cycles were used in order to maintain constant fuel temperatures throughout the process. An amplitude setting of 100% indicates full power.

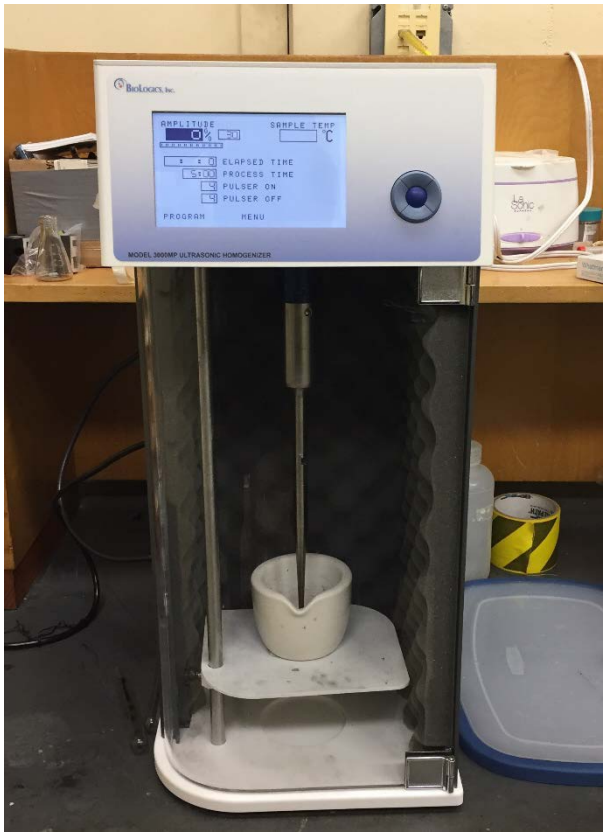

Figure 4.4: Biologics Ultrasonic Homogenizer used to mix Jet-A fuel with nano-additives.

Table 4.1: Homogenizer settings used for mixing CNP.

Setting	Value
Amplitude (%)	100
Process time (Min:Sec)	4:00
Pulsar ON (Min:Sec)	0:10
Pulsar OFF (Min:Sec)	0:10

For MWNTs, the mixing process followed a slightly different track. The fuel – particle combination underwent the mixing parameters outlined in table 4.2. Again, the amplitude was set at 100%, however, the process time was increased from 4 minutes to 20 minutes. The on/off cycles were set at 4 seconds in an attempt to keep the fuel temperature constant throughout the

mixing process. During sonication, fuel temperatures increase as a result of the concentrated energy release the probe creates. By utilizing on/off pulses, the temperature can be maintained and fuel evaporation losses can be reduced. To highlight the importance of surfactant, figure 4.5 shows a CNP fuel sample mixed without the Span 80 surfactant. Note the large clumps and non-uniform consistency. On the contrary, figure 4.6 shows a CNP sample mixed with 1.5% surfactant. Both images were recorded 30 minutes after mixing.

Table 4.2: Homogenizer settings used for mixing MWNT.

Setting	Value
Amplitude (%)	100
Process time (Min:Sec)	20:00
Pulsar ON (Min:Sec)	0:04
Pulsar OFF (Min:Sec)	0:04

Figure 4.5: Jet-A with 0.1% CNP. No surfactant. 30 minutes after mixing.

Figure 4.6: Jet-A with 0.1% CNP, 1.5% surfactant. 30 minutes after mixing.

4.2 Testing Procedure

Tests begun by pressurizing the entire system to 150 psi. This was conducted by gradually increasing the pressure regulator knob on the nitrogen supply tank until the pressure gage on the testing chamber read 150 psi. Once pressurized, the heating system was plugged into the 120 VAC wall outlet. This immediately triggered the heating cable to begin to heat up and activated the temperature monitoring system. On average it took about one hour for the fuel temperature to reach above 300°C. Once the set point of 330°C was reached, the temperature monitor would cut off electricity to the heat cable. Then when the temperature dipped below the set point, electricity would be restored. This led to fuel temperature fluctuations from 300 – 335°C.

Throughout the duration of each test, fuel temperature and pressure was recorded every 10 – 15 minutes. Although the nitrogen pressure supply was never increased, the testing chamber pressure increased slightly as the fuel temperature increased. Typically, this occurred when the liquid fuel in the testing chamber began to run low. In other words, the chamber was filled with more nitrogen gas and fuel vapor and the constant heating led to a pressure rise. Once the pressure started to increase, fuel was added to the system as described in detail in section 4.3.

In order to maintain constant fuel levels inside of the testing chamber, fuel was added periodically. Typically, this procedure was executed every 1.5 – 2 hours. Decreased fuel levels were characterized by increases in the pressure and more rapid temperature changes. The first step for refueling was to close the fuel line valve located between the testing chamber and the pre-heated fuel reservoir. This cut off the nitrogen pressure flow into the chamber. Next, the pre-heated fuel reservoir was depressurized. The regulator valve on the nitrogen tank was first closed, then the relief valve located at the top of the pre-heated fuel reservoir was opened. This

depressurized the vessel and allowed for more fuel to be poured in from the top port. About 500 mL of new Jet-A or nanomaterial fuel was added for each refuel. After the top section was reconnected, the nitrogen regulator was re-opened and the pre-heated vessel was pressurized back up to 150 psi.

Prior to opening the ball valve on the fuel line, the pressurized vapors and waste fuel inside of the testing chamber had to be evacuated. The ball valve on the waste fuel line, below the testing chamber, was opened to allow all of the pressurized vapor and waste fuel to empty out into the waste reservoir. Due to the pressure difference between the two vessels, the contents inside of the testing chamber emptied into the waste reservoir. After a few seconds, the ball valve on the fuel line was then opened; allowing the new Jet-A fuel to flow into the testing chamber. As soon as the flow into the waste reservoir changed from vapor to liquid fuel, the valve on the waste line was closed and the testing chamber was known to be completely filled with new fuel. During refueling, the heating apparatus was not unplugged.

4.3 Post Test Procedures

Following the completion of a test, all vessels were depressurized and the heating apparatus system was stopped. The testing chamber was left to cool under the fume hood with the fan running. After one or two hours, the system had cooled enough to dismantle the setup. First, the testing chamber fuel was emptied by opening the waste reservoir valve. Then, the testing chamber was disconnected from the pre-heated fuel reservoir and the waste reservoir. The aluminum foil, Superwool insulation and the heating cable were all removed from the testing chamber. To unscrew the top section, the chamber was placed in a vice grip, and a wrench was used to pry the top section loose. After which, the stainless steel samples could be collected and

prepared for SEM analysis. Samples were imaged immediately after testing as well as after an ethanol rinse. Ethanol rinses consisted of simply dipping the sample into ethanol to let all un-bonded particulates rinse off.

Results between tests were analyzed and compared through scanning electron microscopy (SEM) images. All imaging was conducted at the Central Microscopy Research Facility, located in the Eckstein Medical Research Building, at the University of Iowa. The microscope used for all samples was the Hitachi S-4800. Due to the sample sizes used for testing, up to three different samples could be loaded in the microscope at a time. The chamber was then closed off and the vacuum pump was activated. The accelerating voltage was set at 10kV and the emission current was set at 10μA for all cases. After alignment and focusing, images were captured at 35x, 1000x, and 5000x magnifications. All data was saved to a portable USB drive to be downloaded to a hard drive later.

4.4 Experimental Issues

While designing the setup and running preliminary tests, some of the issues that arose mainly focused on the refueling procedures and the heating system. Specifically, the first experimental design did not utilize a waste reservoir. Without anyway to empty the vapor contents of the testing chamber, new fuel could not be added to the testing chamber. Essentially, new fuel would remain pressurized in the pre-heated reservoir with no way to flow into the testing chamber, as it was already filled with fuel vapor. This problem was remedied by adding an additional reservoir to the system. This waste reservoir allowed for the internal contents inside of the testing chamber to be released prior to adding more fuel.

The other main issue encountered was with the heating system. This problem was partly a result of the refueling issue and was also fixed by introducing the waste reservoir to the system. Without the additional reservoir, the internal contents of the testing chamber would become primarily filled with stagnate vapors. The lack of flow of the vapor-liquid mixture led to a reduction in convective cooling and subsequently increased temperatures of the testing chamber walls. Initial tests also used temperature settings up to 500°C, which proved to be too high for the system as fuel temperatures would never reach this set point. As a result, the heat cable remained ON for the duration of tests, and as the external wall temperatures increased, the heat cable began to degrade and actually burn in some instances. This problem was fixed by reducing the temperature set point to a more manageable 330°C and by modifying the refueling procedure to be able to cycle in new fuel.

Chapter 5: Results and Discussion

Preliminary testing focused on finalizing an experimental procedure capable of producing coke formation with plain Jet-A fuel. Tests were conducted to fine-tune the heating system, the pressure system, and the refueling procedures described in Chapter 4. After the final design and procedure was completed, testing began in January 2016. A total of thirteen tests were ran from January to April. SEM imaging analysis was performed on five separate stainless steel samples. Of these, two samples were from different plain Jet-A tests, two samples were from different nanoparticle tests, and one sample was from a nanotube test.

5.1 Testing Results

Table 5.1 shows the testing parameters that each test followed. The temperature control device was set at 330°C (626°F) for the duration of tests. However, due to refueling and residual heating and cooling, the actual fuel temperature fluctuated from 300°C – 350°C. Figure 5.1 shows the internal fuel temperature with respect to time for each test with which samples were imaged. All tests were run for approximately 6 hours. On average, it took one hour for the internal fuel temperature to rise above 300°C. All tests followed the same temperature ramp up and fluctuation behavior outlined in figure 5.1.

Table 5.1: Testing parameters.

Internal Fuel Temperature (°C)	330
Wall Temperature (°C)	425
Pressure (Bar)	10

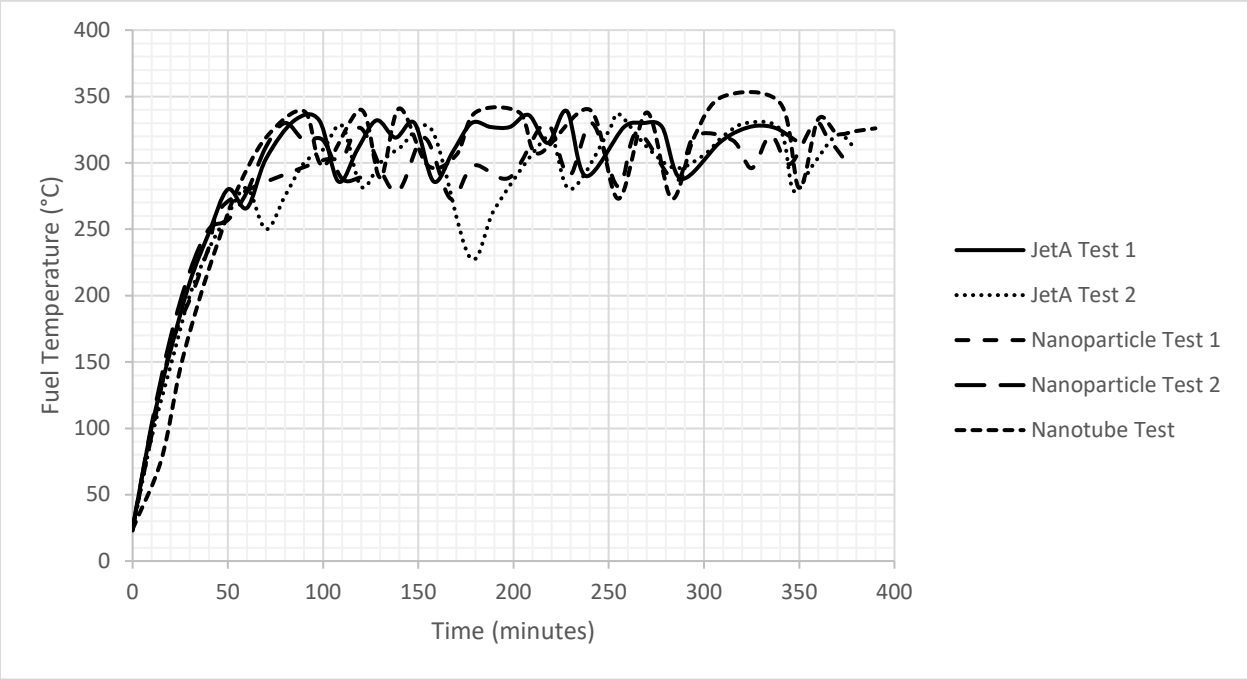

Figure 5.1: Fuel temperature vs. time.

Figures 5.2 – 5.4 show a plain sample, a nanoparticle sample, and a Jet-A sample respectively. Comparing the three, it can be seen that the Jet-A sample appears to have significantly more particulates bonded to the top surface than the other two. The nanoparticle sample more closely resembles the plain sample. However, in order to more accurately quantify the amount solid deposits, SEM analysis was conducted.

Figure 5.2: Plain sample.

Figure 5.3: Nanoparticle samples.

Figure 5.4: Jet-A sample.

5.2 SEM Image Results

Scanning electron microscopy analysis was used to examine the surface of the stainless steel samples between the different tests. For each sample, images were recorded at 35x, 1000x, and 5000x magnifications (see the Appendix for 5000x). Figures 5.5 and 5.6 display the surface of a plain stainless steel sample at 30x and 1000x magnifications respectively. It can be noted that the surface at 30x magnification has smooth and rough areas due to the machining process. It's important to note that all samples exhibit the same rough and smooth surface qualities. The 1000x magnified image highlights how a deposit free surface appears when magnified. Note, the surface is smooth and relatively uniform. There are no discontinuities or added particles.

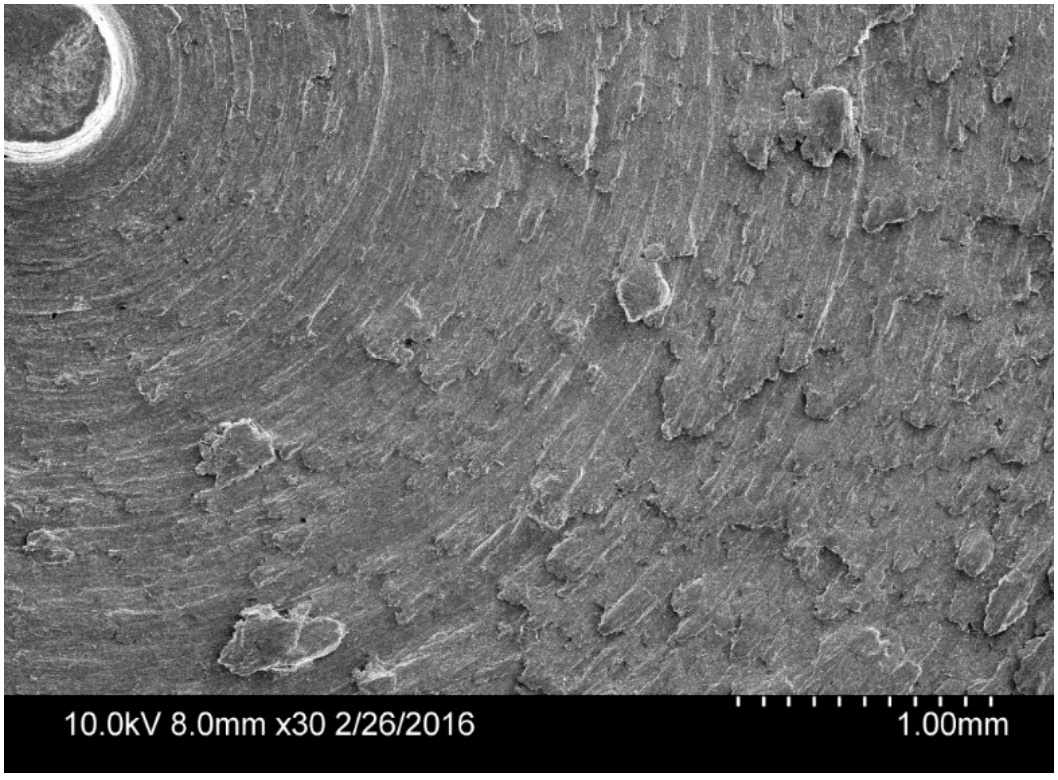

Figure 5.5: Plain sample, 30x.

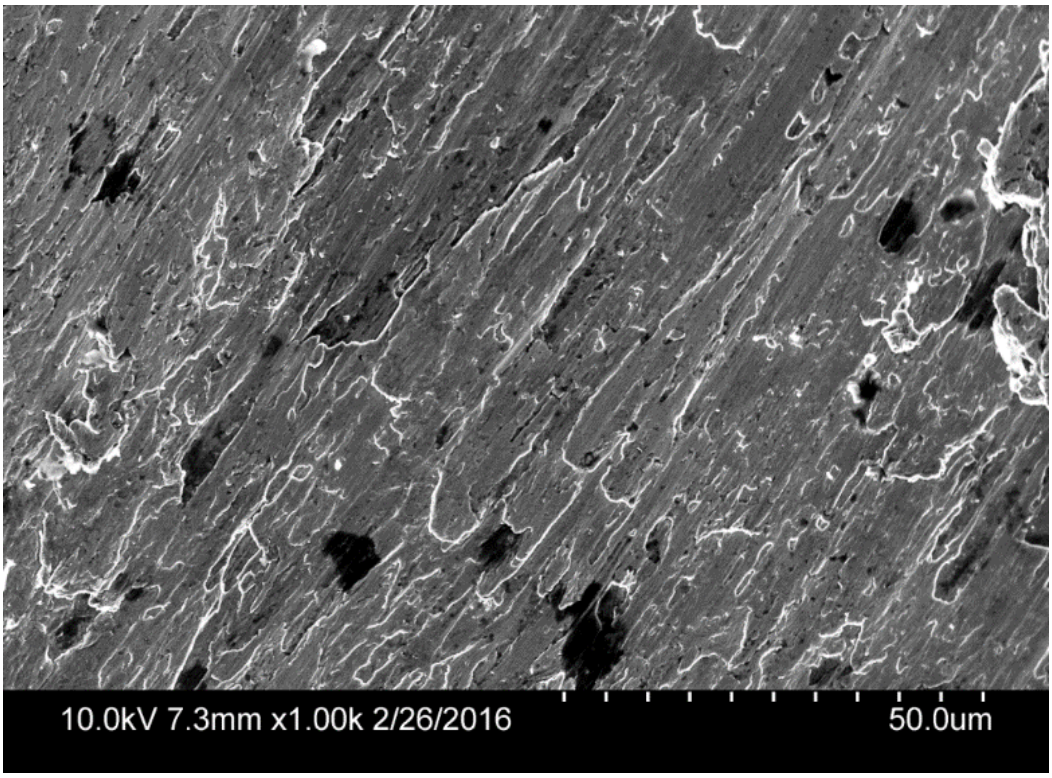

Figure 5.6: Plain sample, 1000x.

The next series of images are from plain Jet-A fuel tests. These samples were run using the experimental setup and procedures described in Chapters 3 and 4. Figures 5.7 – 5.10 show the results from two separate Jet-A tests at 35x and 1000x magnifications. The appendix provides images at 5000x magnifications. Analyzing the differences between the plain and Jet-A samples at 35x magnification, there are significantly more particulates (black specs) bonded to the stainless steel surface. When magnified to 1000x, it becomes even more evident that both Jet-A tests yielded significant deposit formation and surface bonding. These results are amplified when compared to the smooth surface in figure 5.6. It is important to note that all of the samples displayed below were imaged prior to an ethanol rinse.

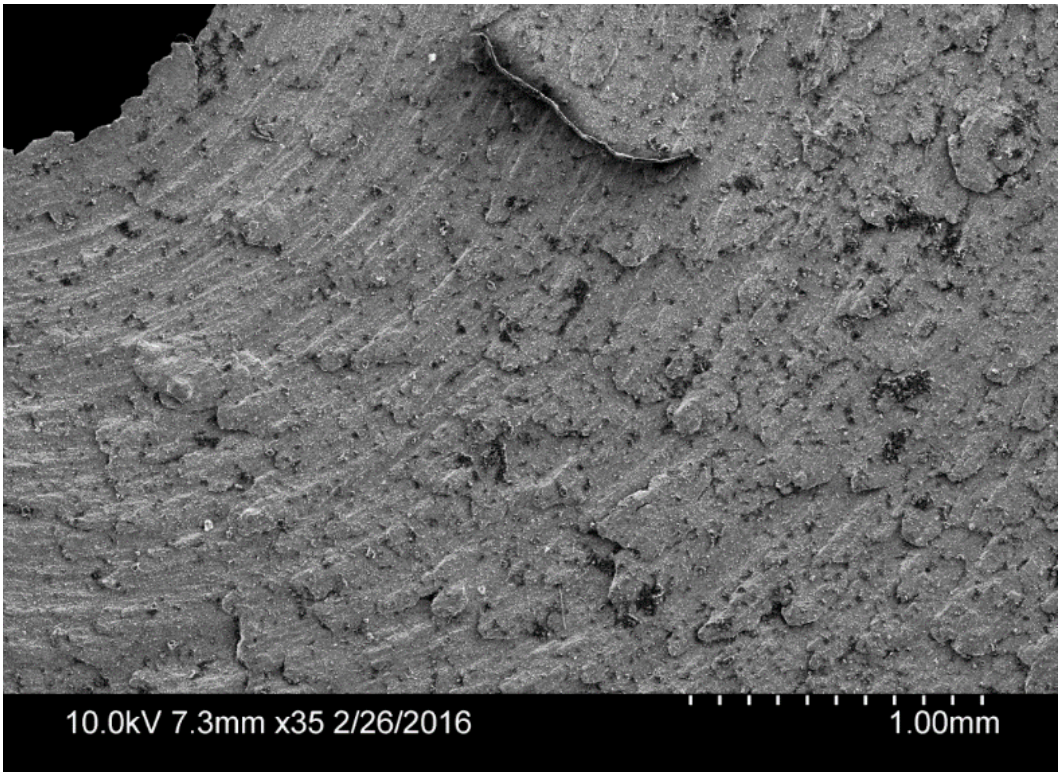

Figure 5.7: Jet-A sample 1, pre-ethanol, 35x.

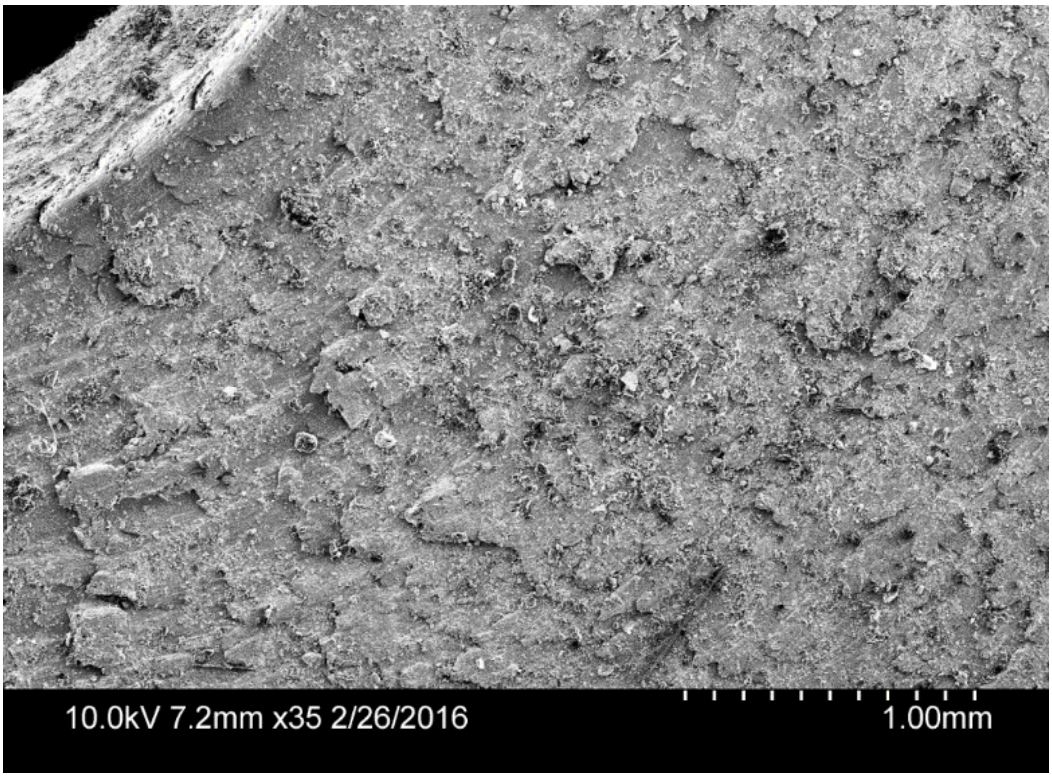

Figure 5.8: Jet-A sample 2, pre-ethanol, 35x.

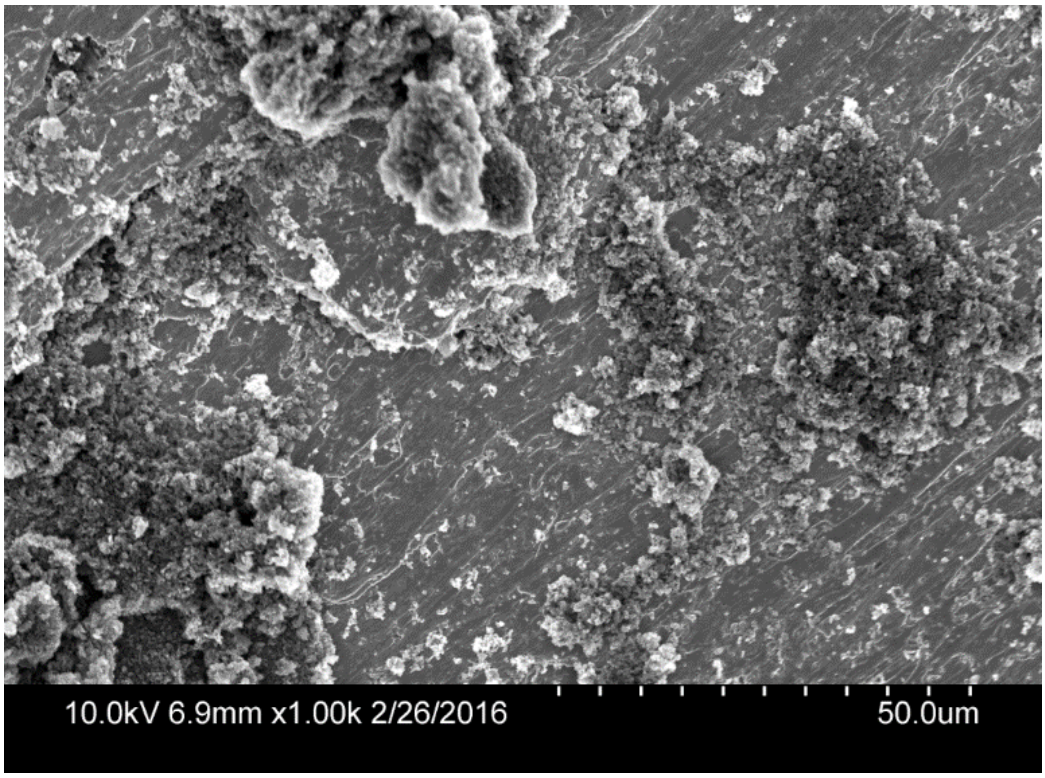

Figure 5.9: Jet-A sample 1, pre-ethanol, 1000x.

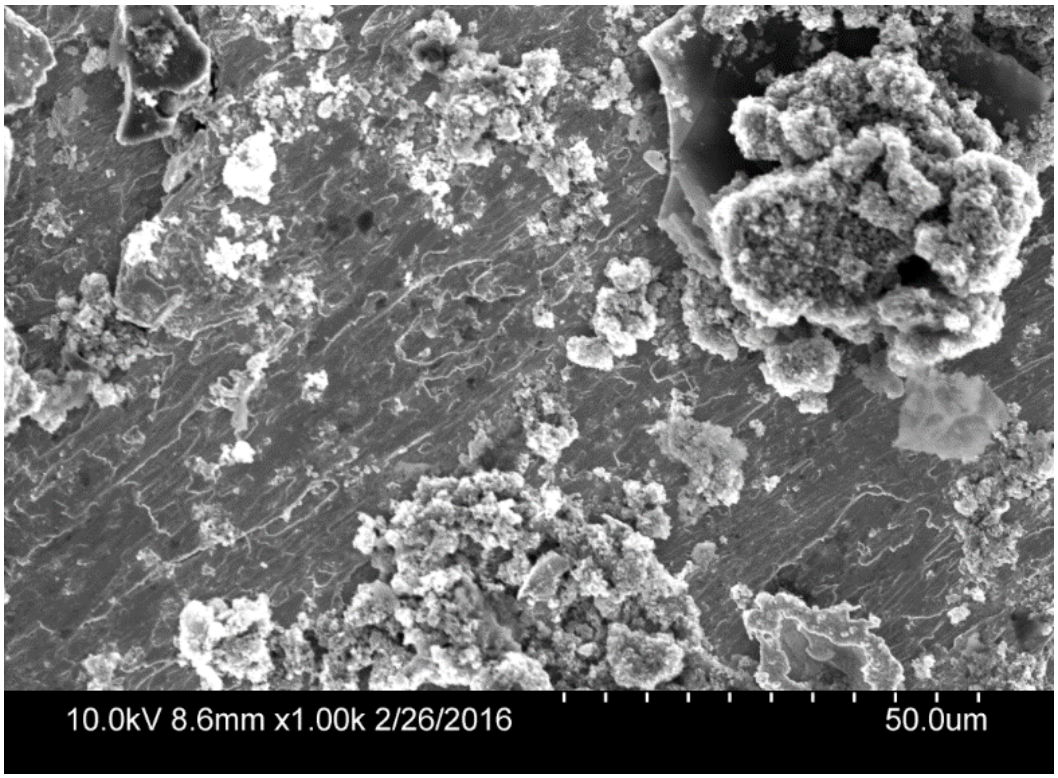

Figure 5.10: Jet-A sample 2, pre-ethanol, 1000x.

Figures 5.7 – 5.10 confirm that the experimental setup and procedure utilized was effective for simulating coke deposit formation and build up on stainless steel surfaces. The next tests were conducted under the same conditions with Jet-A fuel mixed with 0.1% carbon nanoparticles. This mixture was generated as described in section 4.1.1. Figures 5.11 and 5.12 display the first nanoparticle sample at 35x and 1000x magnifications. Immediately, it can be seen that the surface of the 35x image is covered in black material. These samples were also not rinsed in ethanol prior to being imaged. They were extracted from the testing apparatus and simple left to air dry. As a result of adding the carbon particles to the fuel, the color became a dark black, which consequently led to a dark residue left over on the sample surface if left to air dry. Thus, the dark residue was believed to only be a result of the fuel residue, and not bonded particulates. Furthermore, the 1000x magnified image in figure 5.12 reveals much smaller particle size than seen in figures 5.9 and 5.10.

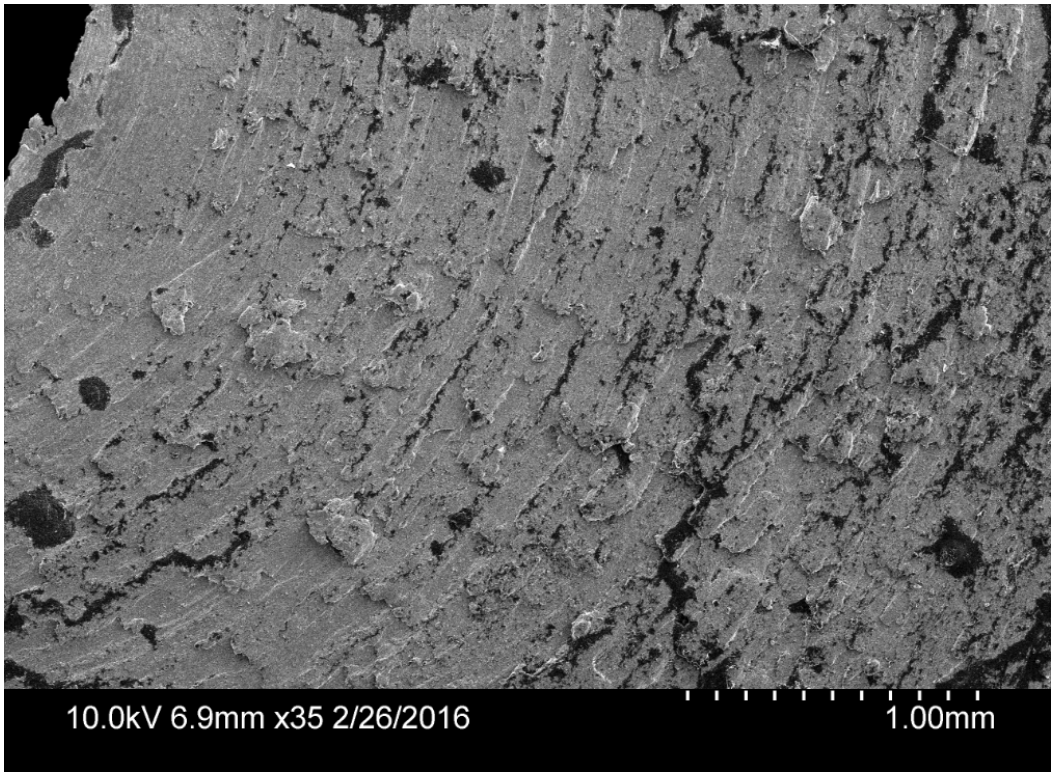

Figure 5.11: Nanoparticle sample 1, pre-ethanol, 35x.

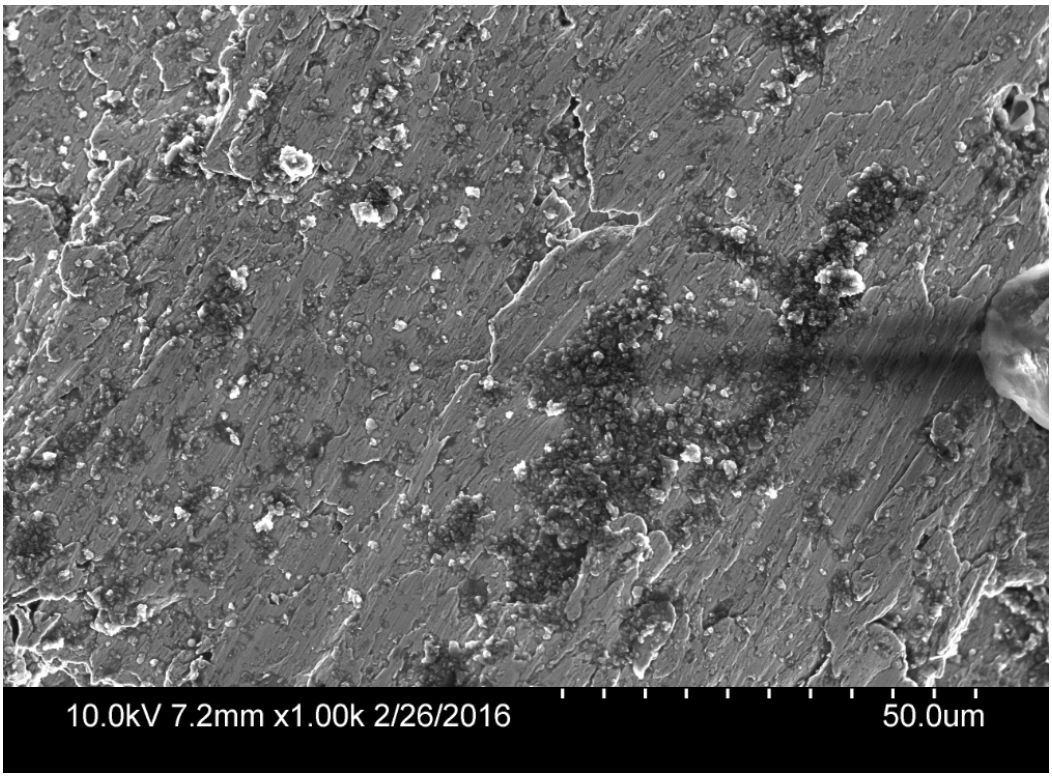

Figure 5.12: Nanoparticle sample 1, pre-ethanol, 1000x.

After examining the results, the particle size and formation on the 1000x magnified images revealed significantly less deposits on the nanoparticle sample compared to the normal Jet-A fuel tests. However, the next step was to determine if the black coloring on the nanoparticle sample was only a residue or bonded material (i.e. coke deposits). All samples were dipped in ethanol to remove all un-bonded particulates from the surface. Each sample was re-imaged and can be viewed below in figures 5.13 – 5.18. These results proved to be extremely positive. Figures 5.13 – 5.16 show the Jet-A samples after the ethanol rinse, and it can be seen that the majority of the bonded particulates remained on the surface. There are still ample deposits over the entire surface. Figures 5.17 and 5.18 show the nanoparticle sample after the ethanol rinse, and in both magnifications, it can be seen that all of the black residue left over on the surface was washed off by simply dipping the sample in ethanol.

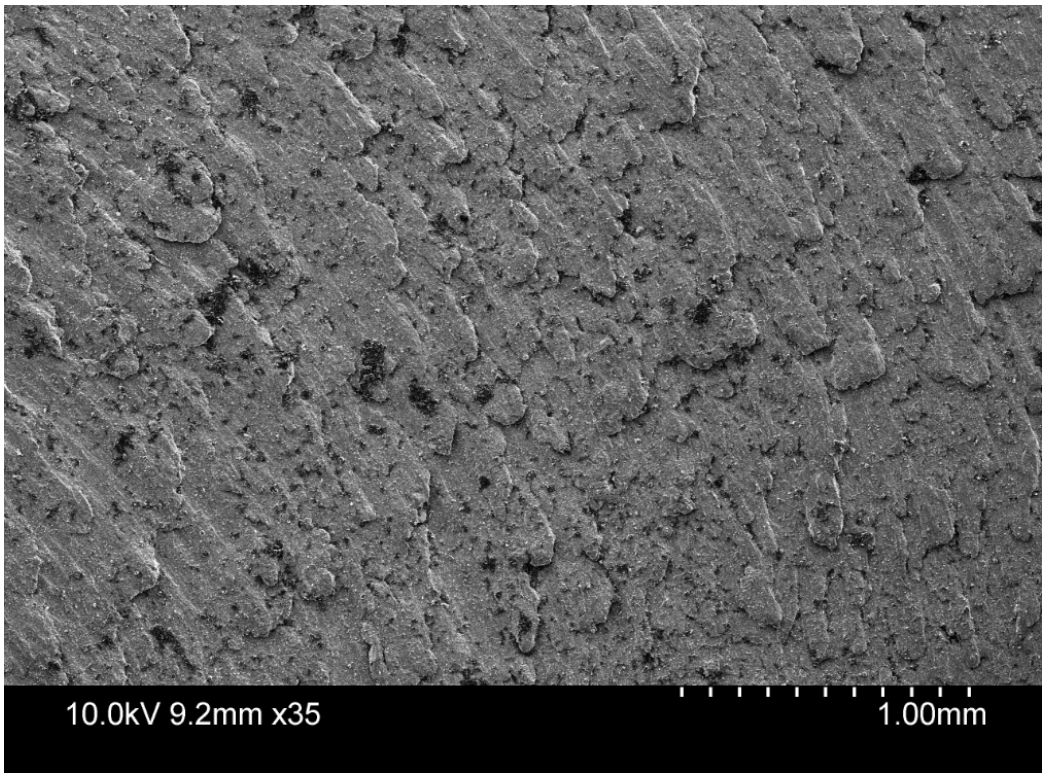

Figure 5.13: Jet-A sample 1, post-ethanol, 35x.

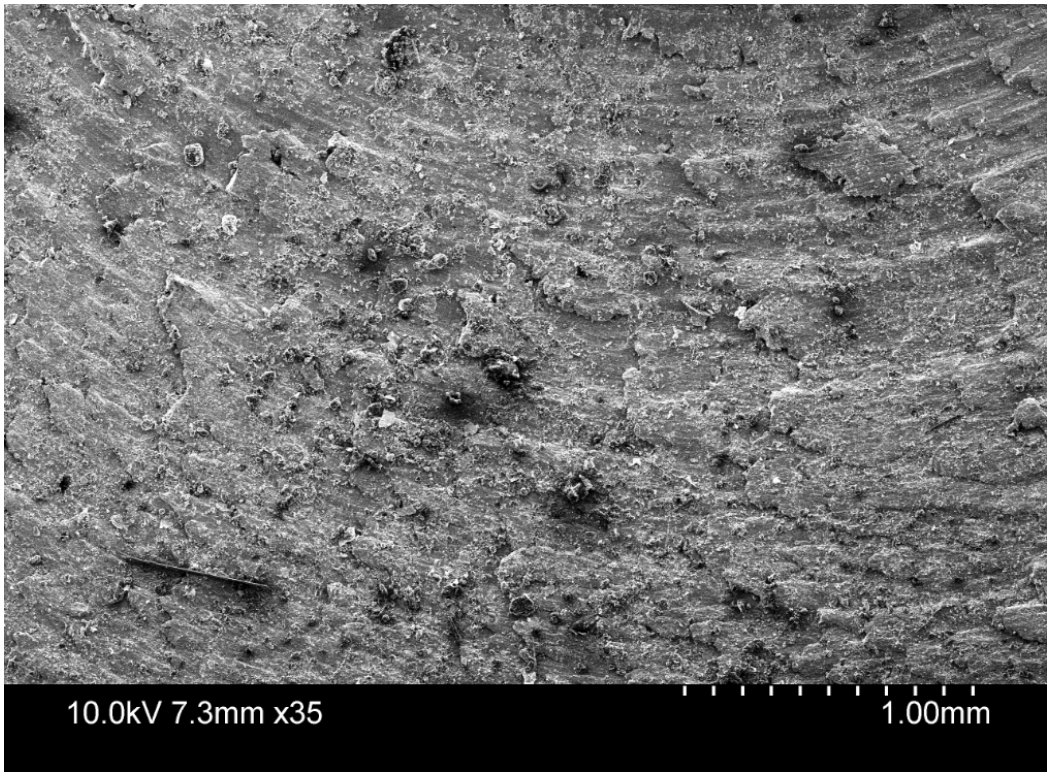

Figure 5.14: Jet-A sample 2, post-ethanol, 35x.

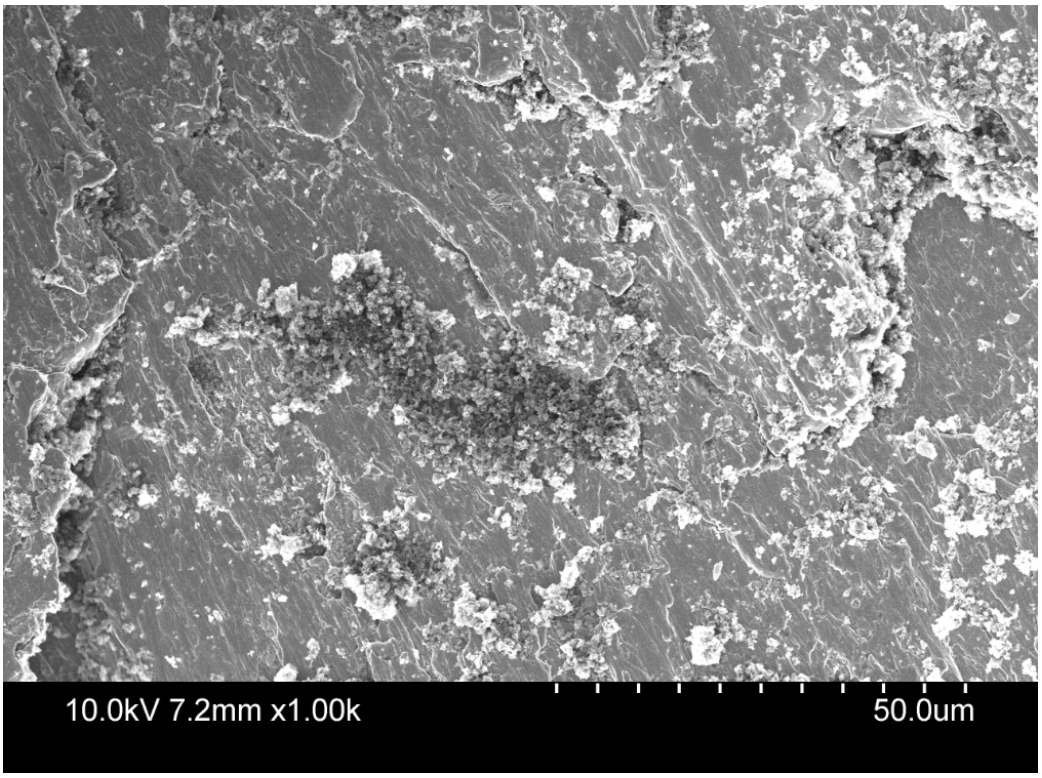

Figure 5.15: Jet-A sample 1, post-ethanol, 1000x.

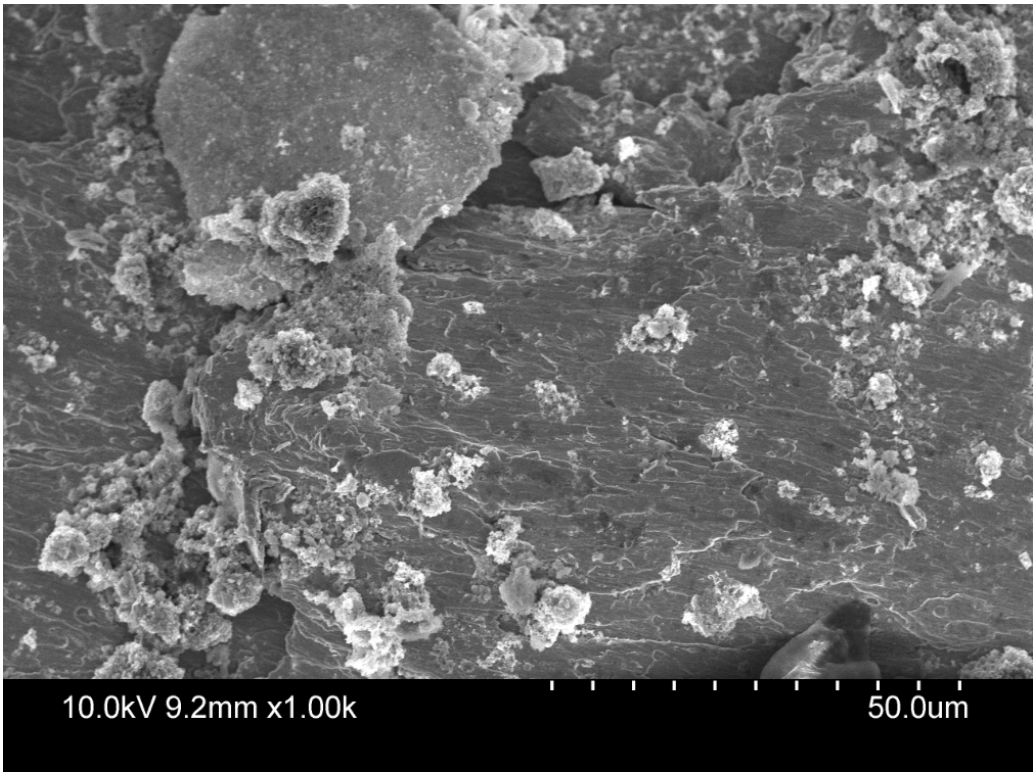

Figure 5.16: Jet-A sample 2, post-ethanol, 1000x.

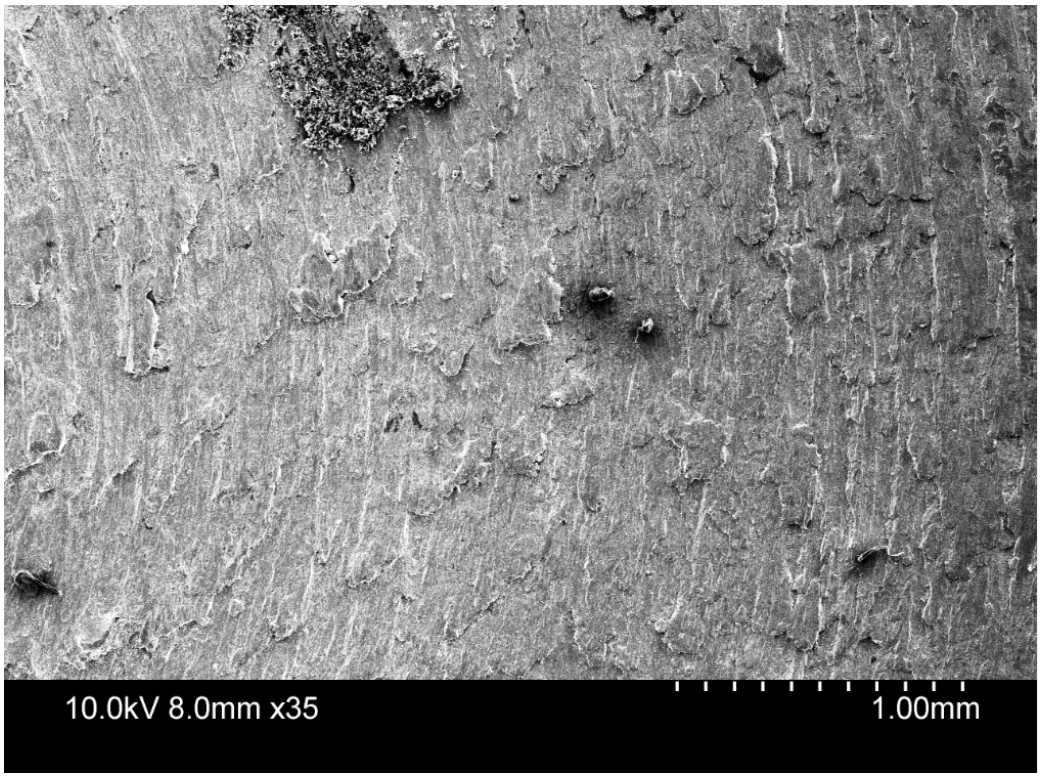

Figure 5.17: Nanoparticle sample 1, post-ethanol, 35x.

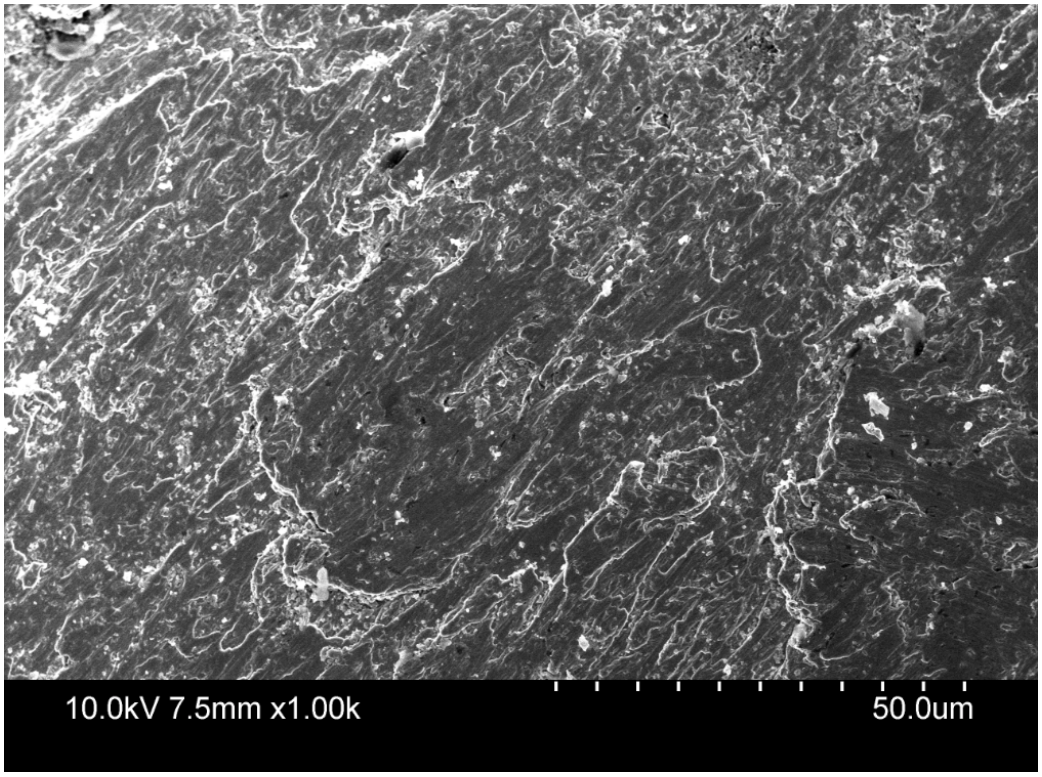

Figure 5.18: Nanoparticle sample 1, post-ethanol, 1000x.

Tests continued using the 0.1% nanoparticle and Jet-A mixture. Figures 5.19 and 5.20 show the pre-ethanol rinse SEM image results. Similarly, the same black coloring formed on the surface as a result of the fuel residue drying. Taking a closer look at figure 5.20 shows very minimal particle formation similar the results from the first nanoparticle test in figure 5.12. Although the surface is not as smooth as the plain stainless sample, the particle size and distribution is considerable less than the Jet-A samples, thus indicating minimal coke build up. The sample was then rinsed in ethanol and re-imaged. Figures 5.21 and 5.22 show the 35x and 1000x magnifications respectively. After the rinse, the majority of fuel residue washed off and the 1000x magnified image shows a little more particle formation than the previous nanoparticle sample (figure 18). The particle size and distribution is still much less than the Jet-A samples.

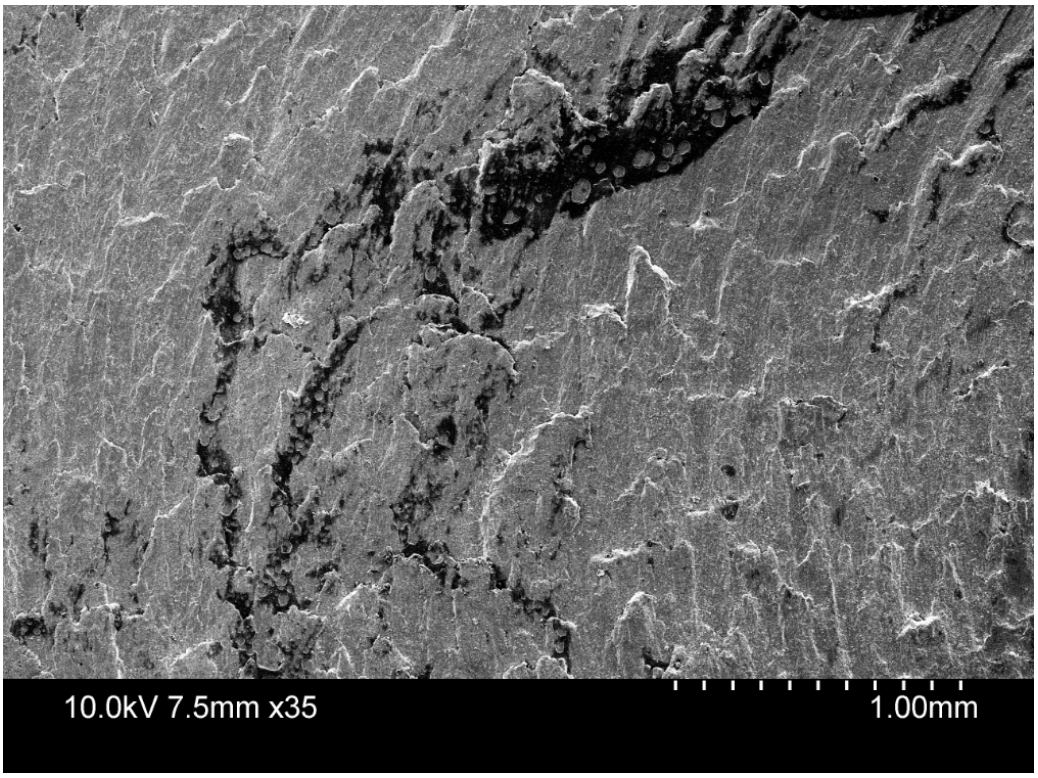

Figure 5.19: Nanoparticle sample 2, pre-ethanol, 35x.

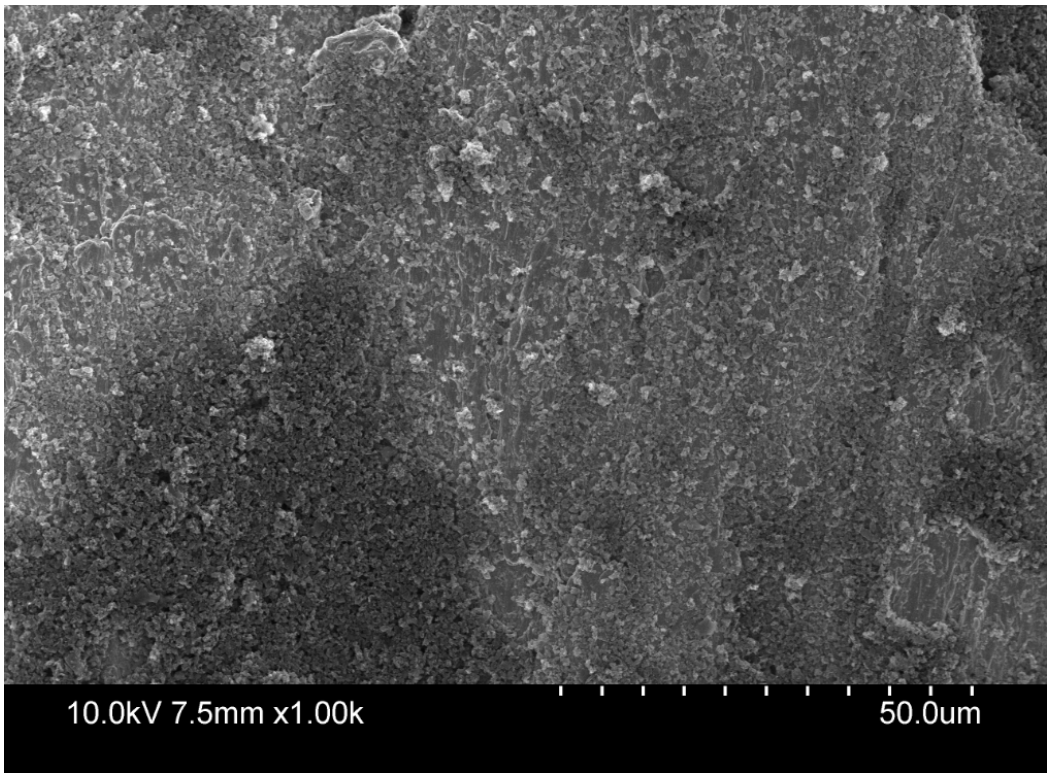

Figure 5.20: Nanoparticle sample 2, pre-ethanol, 1000x.

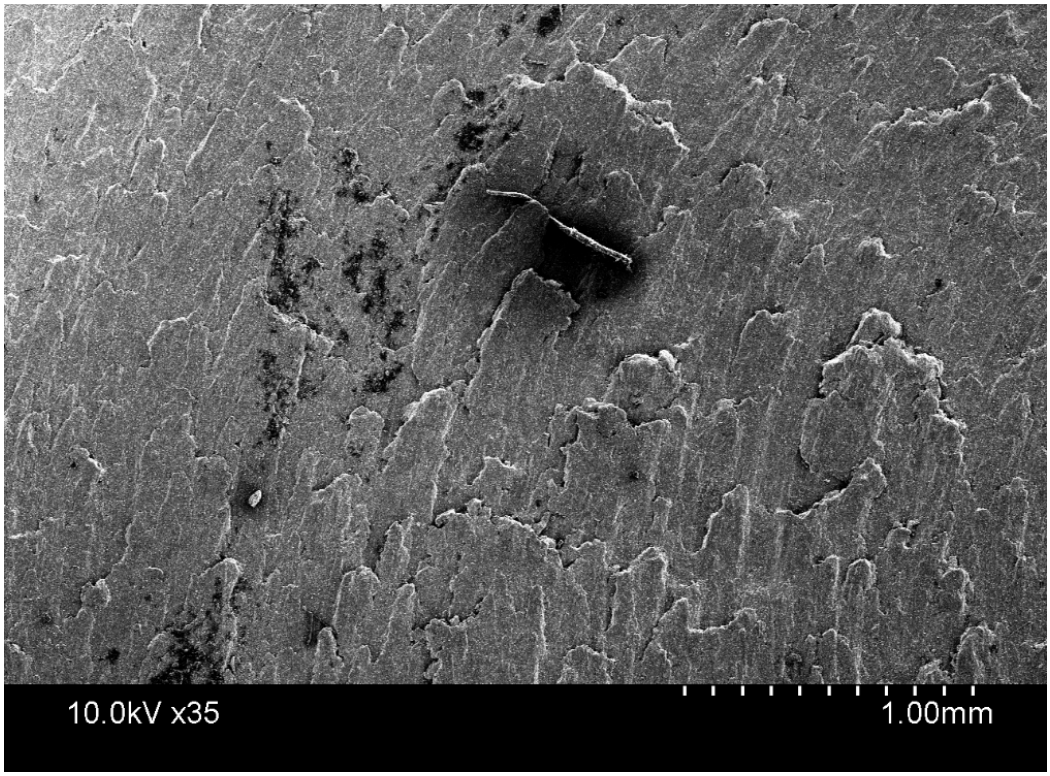

Figure 5.21: Nanoparticle sample 2, post-ethanol, 35x.

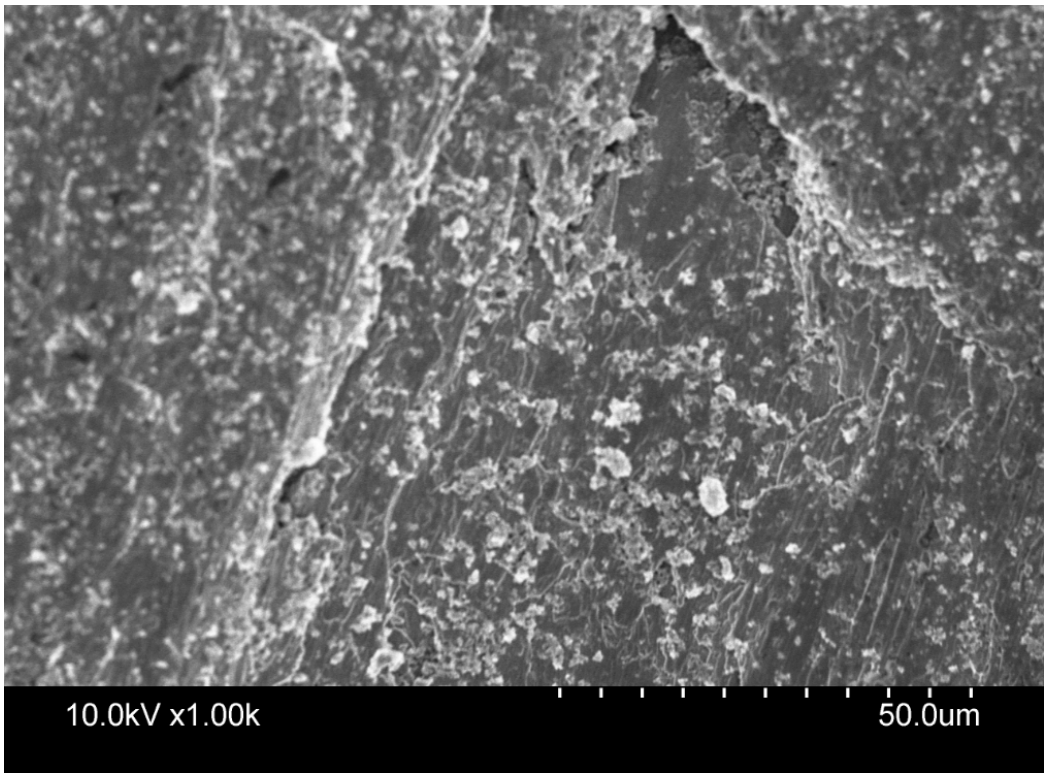

Figure 5.22: Nanoparticle sample 2, post-ethanol, 1000x.

The last tests conducted utilized MWNTs (nanotubes) as the fuel additive instead of CNPs (nanoparticles). As stated previously, the carbon nanotubes had diameters ranging from 8-15 nm and lengths from 0.5-2 μm. Compared with the 100 nm diameter particles used in the previous two tests, the nanotubes are larger, and thus provide a greater surface area for particulates to bond too. Figures 5.23 and 5.24 show the ethanol rinse images from the nanotube test. Results can be seen to be very similar to the nanoparticle tests. There was again minimal deposit formation and bonding to the surface.

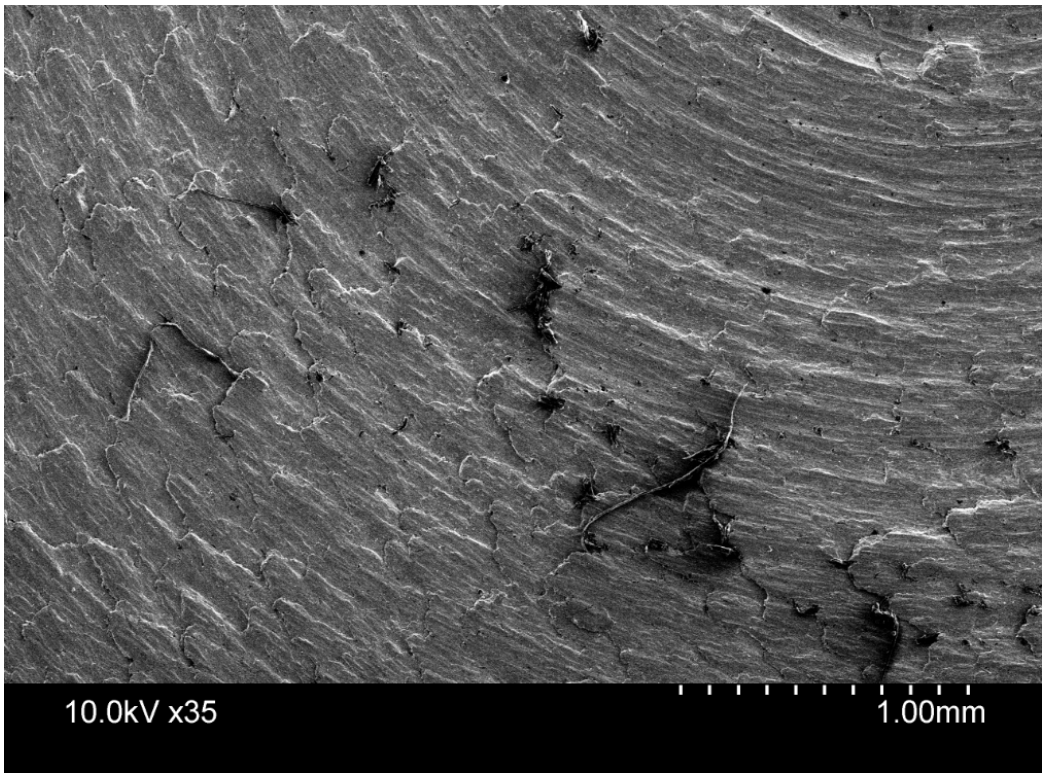

Figure 5.23: Nanotube sample 1, post-ethanol, 35x.

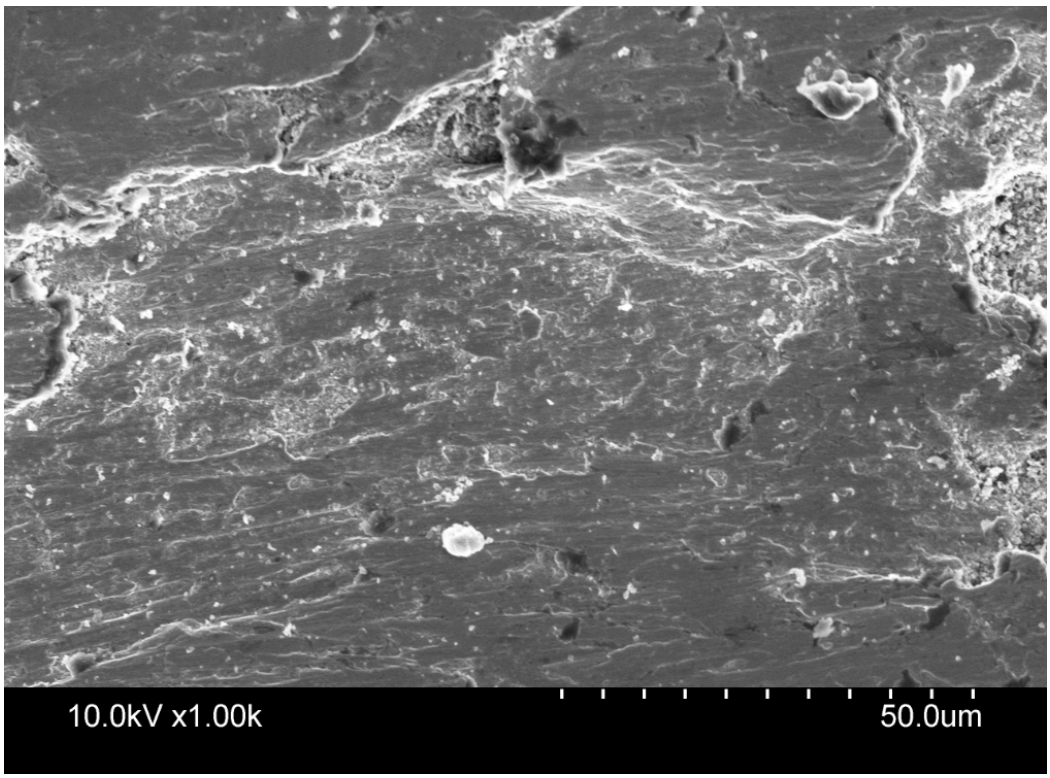

Figure 5.24: Nanotube sample 1, post-ethanol, 1000x.

5.3 Discussion

SEM analysis clearly demonstrated that nanoparticle and nanotube fuel additives have a positive effect on reducing deposit build up on stainless steel surfaces. In addition, comparing the pre and post ethanol rinse images between the Jet-A and nanomaterial samples revealed that the nanoparticle samples contained minimal bonded deposits. In all cases, the dark fuel residue was completely rinsed off and any particle formation on the surface was dramatically reduced compared to the Jet-A samples. Undergoing the same procedure, the Jet-A deposits remained in size and distribution throughout the surface, underscoring that these deposits were physically bonded to the surface rather than just a left over residue as a result of fuel drying on top of the sample.

The next question is why did the carbon nanoparticles and nanotubes have such a profound impact on reducing deposit formation. This question is not easily answered, as it is not fully known. As stated in Chapter 2, the chemical mechanisms that describe coking are very complex, and research is still being conducted to better understand the kinetics. However, a couple theories exist that could help better explain this mechanism.

The first theory is that the particles provided preferred nucleation sites for the deposits to bond too. During nucleation, the surface of a different substance acts as the center for the atoms and molecules of the deposit to form [12]. In other words, the actual coking mechanism was not halted, but rather the deposit byproducts bonded to the particles instead of the stainless steel. As highlighted in Chapter 2, Kendall and Mills hypothesized that stainless steel could act as a catalyst for deposits to form [11]. Specifically, the chemical composition of stainless steel was found to be more favorable for deposit formation than aluminum and other metals. The addition of carbon particles in the fuel may have provided an equally favorable nucleation site for the

deposits to bond too. Fuel directly in contact with the stainless steel could still result in bonded particulates forming on the surface. However, thermally stressed fuel away from the stainless steel would form deposits onto the local nanoparticles. The resulting nanoparticle – deposit combination would simply follow the bulk flow of the fuel and not bond to the stainless steel surface. This was demonstrated in each of the nanoparticle – nanotube tests where the pre-ethanol rinse images showed a dark fuel residue left over on the surface. After a light ethanol rinse of each sample, the residue was completely removed, indicating the majority of the particles on the surface were not bonded. Rather, these particulates were a combination of the nanoparticles and solid deposits formed away from the stainless surface. At the conclusion of a test, while the fuel was left to cool, these particles settled on top of the stainless samples instead of actually bonding to the surface as seen in the normal Jet-A fuel tests. As a reminder, the same procedure was carried out with the Jet-A samples, and the post-ethanol rinse images still contained a significant amount of deposits. This indicated that these deposits were actually bonded to the stainless steel surface, instead of just being left over.

Another explanation for the positive results could have been that the nanoparticles did in fact have an effect on the chemical coking mechanism. As highlighted in section 2.2.1, fuels that oxidize more easily were found to be thermally stable and produced less deposits [6]. On the other hand, thermally unstable fuels were found to contain added impurities that slowed oxidation. The addition of carbon nanomaterial may have had an effect on reducing the impact that impurities have on the autoxidation reactions. Thus, fuel with nanomaterial additives may have oxidized easier than plain Jet-A fuel, and as a result, less solid deposits formed.

5.4 Uncertainty Analysis

Uncertainty and error sources are prevalent during any experimental procedure or process. Specific sources of error in this experimental study mainly arose from temperature and pressure monitoring. For the temperature monitoring system, the control device had a small output resolution of ±0.5°C, while the K-type thermocouple had an error of ± 2°C [17]. In addition, the temperature was recorded at the exact center of the testing chamber, while the stainless steel samples were located at the bottom. It was assumed that the fuel temperature at the bottom of the chamber would be the same as at the center. Also, the testing chamber wall temperature was measured on the outside of the chamber, instead of the inside. With insulation surrounding the exterior of the chamber, the heat flux leaving the chamber was assumed to be zero. Hence, the temperature on the outside wall would closely match the inside wall temperature. Although some of these assumptions only provide approximations, they are still valid enough to be able to provide close approximations to the actual temperatures. In order for fuel degradation to occur, temperatures exceeding 300°C would be sufficient. Thus, extremely precise fuel temperatures were not required. Based off the low uncertainty of the thermocouple and temperature control device, as well as the valid assumptions, the temperature monitoring technique was determined to be accurate for testing as long as the same equipment and settings were used for each test.

Pressure monitoring was another relatively small source of uncertainty. The pressure regulator valve on the nitrogen supply was set to 150 psi (10.3 Bar), and pressure was monitored from the gage on the testing chamber. This gage had a resolution of ± 1 psi. Similar to temperature, the if the pressure of the fuel was kept within one psi of the 150 psi set point for each test, results would remain valid.

Chapter 6: Conclusion

6.1 Conclusion

An experimental setup and procedure was designed to thermally stress Jet-A fuel. This setup simulated autoxidation reactions that would occur in a real jet engine application in order simulate fuel degradation, or coking. Specifically, fuel was pressurized to 10 Bar heated to 330°C for durations up to 6 hours. Experiments were conducted using plain Jet-A fuel and Jet-A fuel with 0.1% carbon nanoparticle and nanotube additives. Deposit formation and build up on stainless steel surfaces was analyzed using scanning electron microcopy imagery. Results indicated that the addition of carbon nanomaterial in the fuel led to a reduction in the amount of bonded deposits that formed on stainless steel. There was a significant reduction in particulate size and distribution between the plain Jet-A samples and the nanomaterial samples. Pre and post ethanol rinse images further underscored these results. Post-ethanol rinse Jet-A samples maintained an even distribution of solid deposits, while post-ethanol rinse nanomaterial samples yielded a large reduction in deposits; thus indicating the particulates were not bonded to the surface.

Two different types of nanomaterials were tested in order to determine if one was better than the other. In these preliminary tests, both the CNPs and MWNTs proved to be effective against coke build up. It is difficult to say whether one nano-additive was better than the other under the tested conditions. Although MWNTs are more complex and expensive than CNPs, they have a greater surface area, which may play an important role in suppressing coke build up. As stated in section 5.4, the actual mechanism at play here is not fully know. However, if the first theory is true, and the nano-additives provide preferred nucleation sites for deposits to form,

a greater surface area would provide larger nucleation sites away from stainless steel wall surfaces. Theoretically, this could lead to an even greater reduction in coke deposit buildup.

6.2 Future Work

This study provided a preliminary look into the effect nanomaterials could have on reducing coke build up. Although results proved to be promising, there is still a great deal of work required to further solidify the results. Specifically, fuel temperatures and pressures need to be increased. Wall temperatures can reach as great as 900 K and pressures as high as 100 Bar in a real jet engine application. Increased temperatures and pressures subsequently decrease the residence times as well. Moving forward, modifications need to be made to the testing setup to allow for more extreme temperatures and pressures and shorter tests. Specifically, utilizing a high temperature oven as the heat source could provide enough heat to the system to achieve these temperatures. In addition, other fuels should also be tested to see if the nanomaterials have the same effect or not.

If future tests can be run at greater temperatures, coking will be characterized by the pyrolysis mechanism, and thus larger deposits will form compared to the autoxidation mechanism tested in this report. With larger deposit rates, MWNTs may prove to be more effective against deposit build up, as they have a greater surface area than CNP. If true, the theory that the nanomaterial provides preferred nucleation sites may be validated and the actual coke suppressing mechanism could be better understood for future applications.

Appendix: SEM images at 5000x

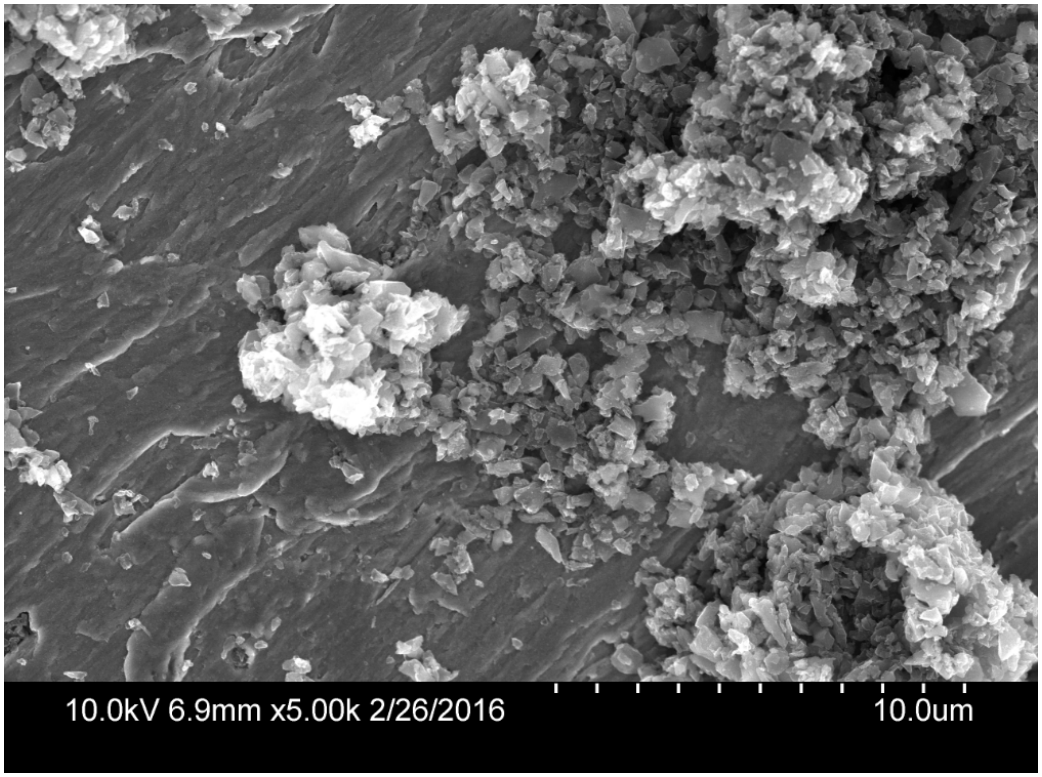

Figure A.1: Jet-A sample 1, pre-ethanol, 5000x.

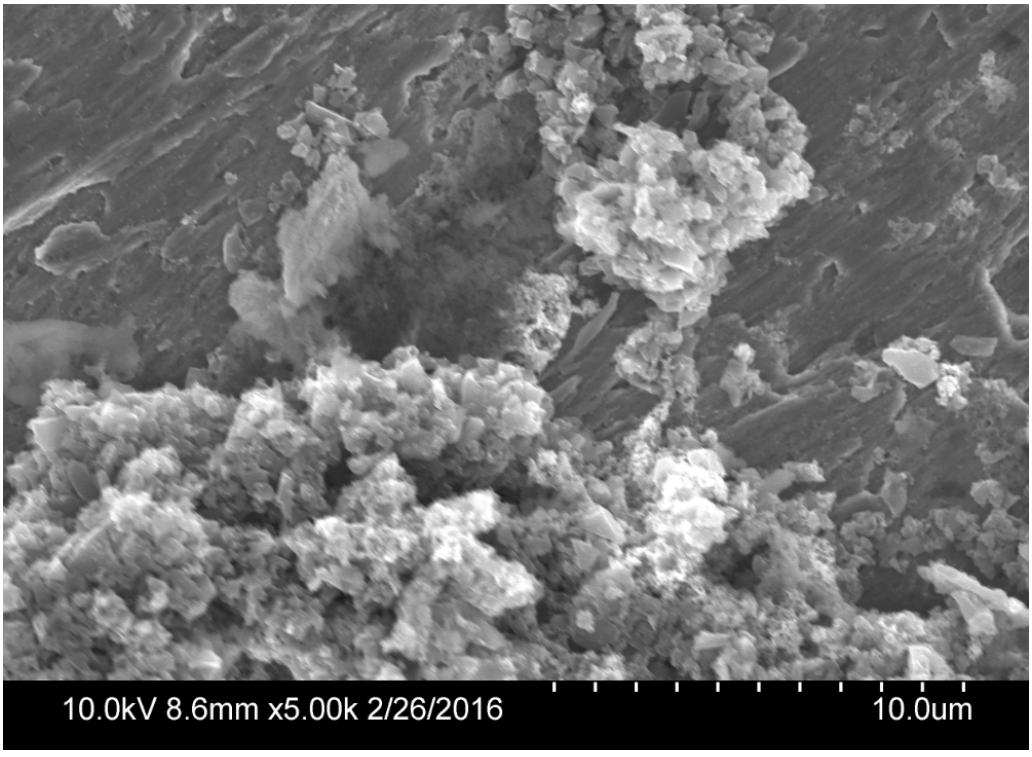

Figure A.2: Jet-A sample 2, pre-ethanol, 5000x.

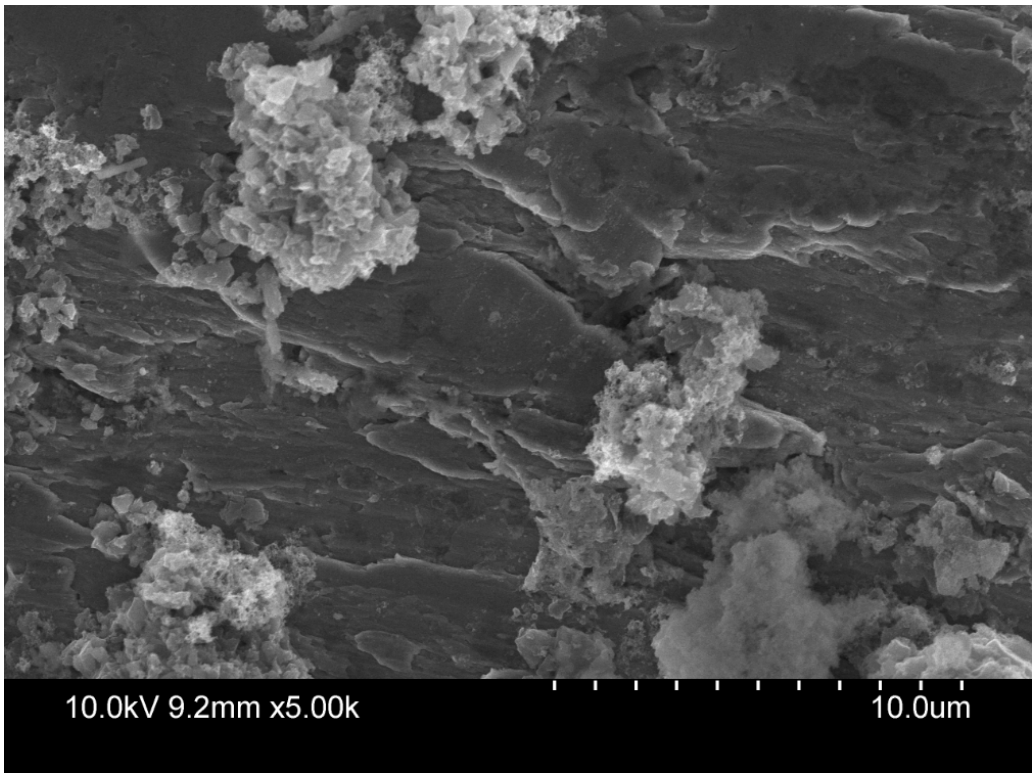

Figure A.3: Jet-A sample 2, post-ethanol, 5000x.

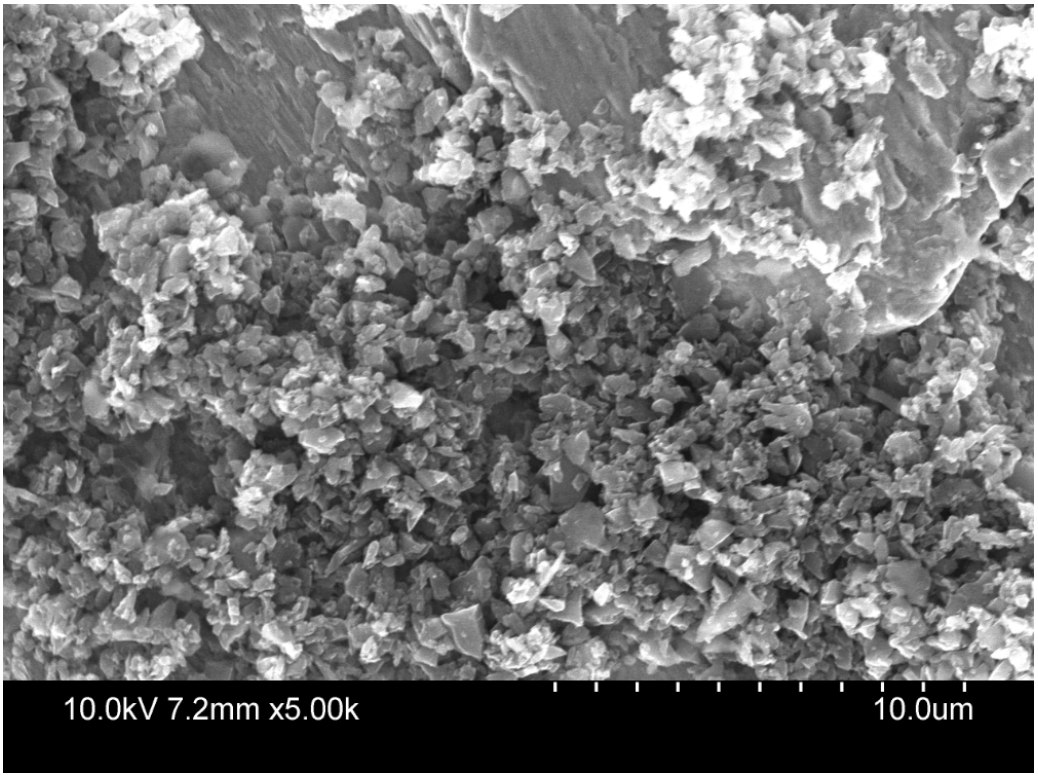

Figure A.4: Jet-A sample 1, post-ethanol, 5000x.

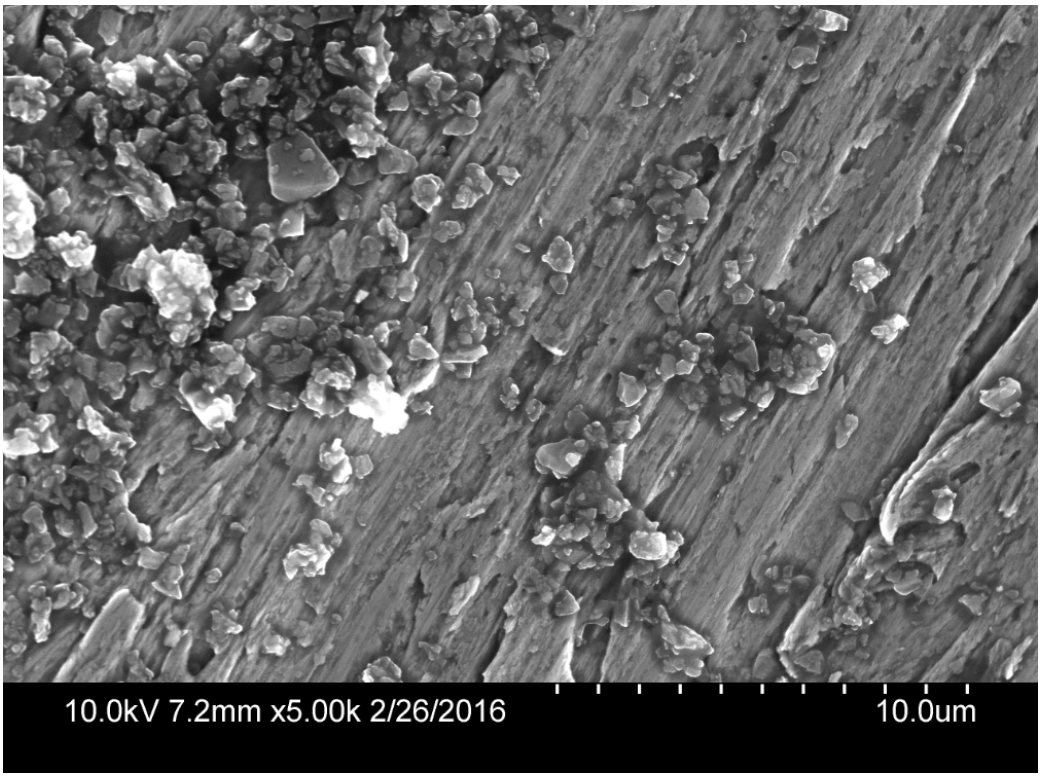

Figure A.5: Nanoparticle sample 1, pre-ethanol, 5000x.

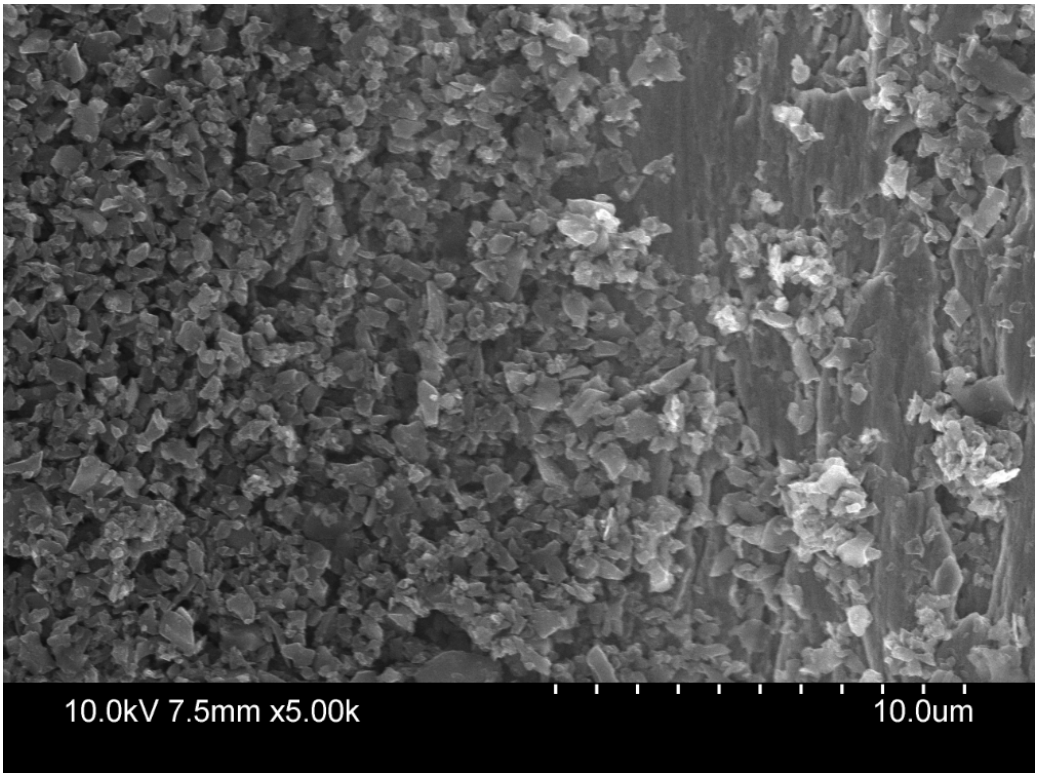

Figure A.6: Nanoparticle sample 2, pre-ethanol, 5000x.

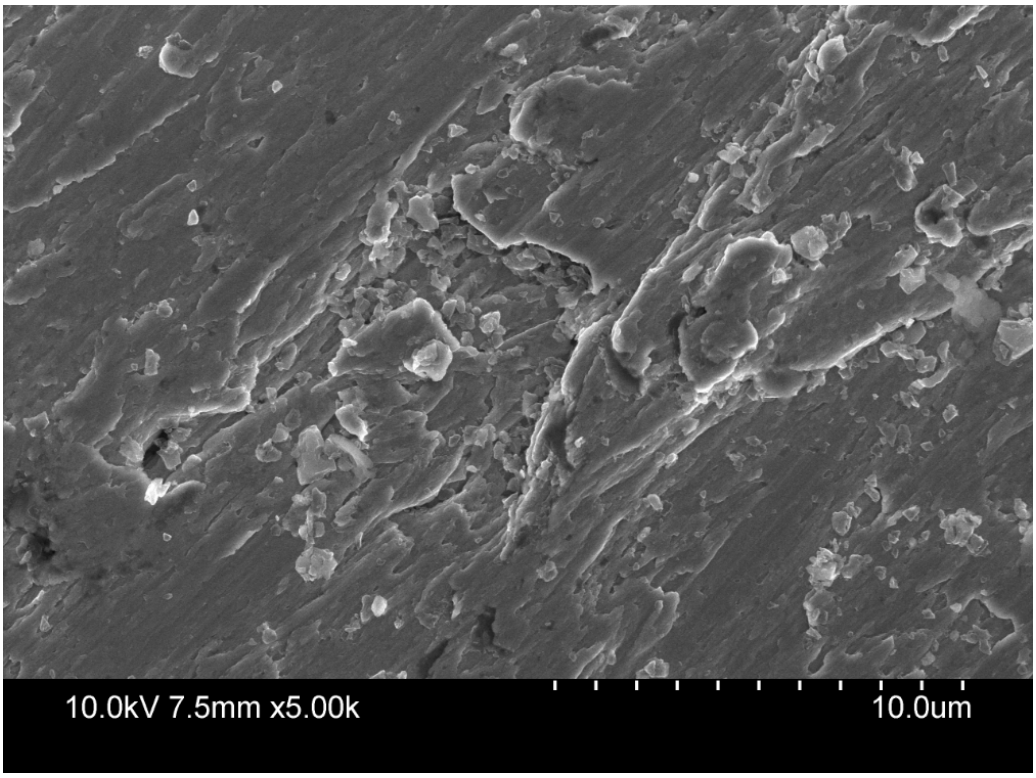

Figure A.7: Nanoparticle sample 1, post-ethanol, 5000x.

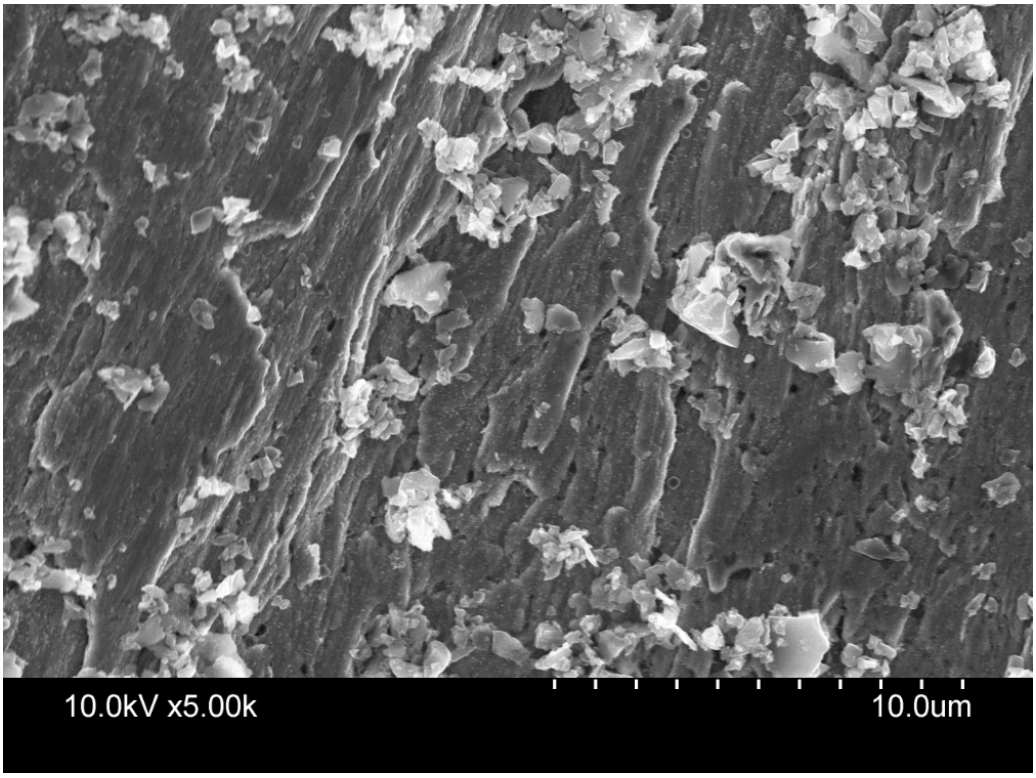

Figure A.8: Nanoparticle sample 2, post-ethanol, 5000x.

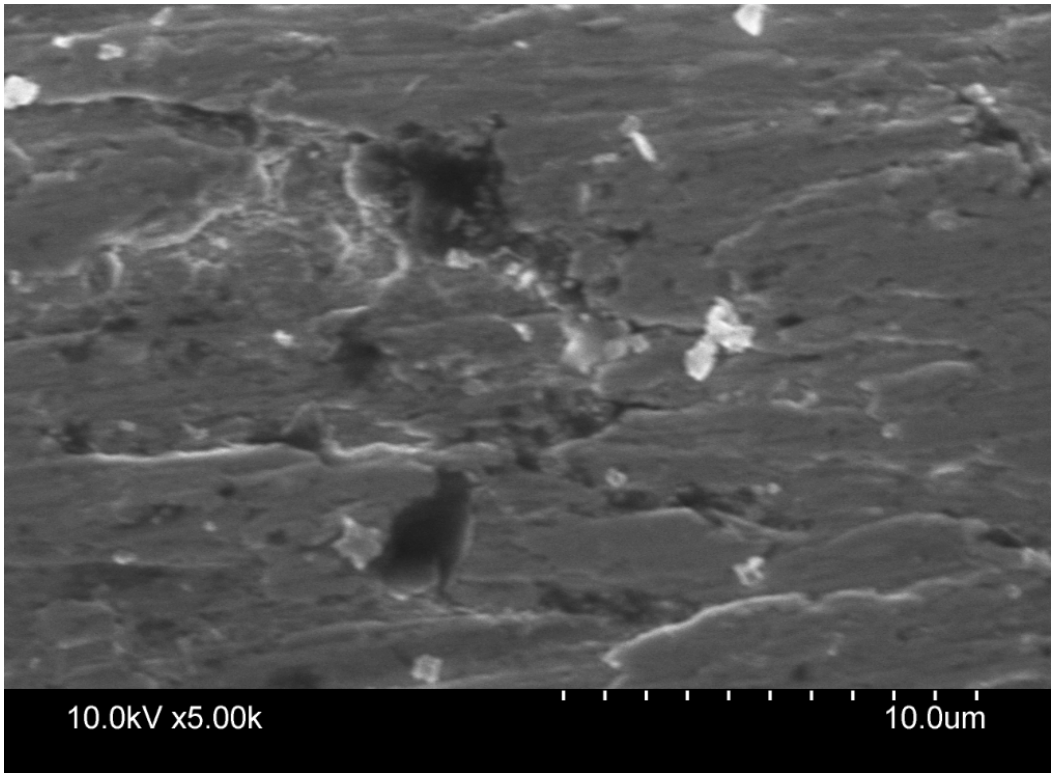

Figure A.9: Nanotube sample, post-ethanol, 5000x.

References

[1] Altin, O. and Eser, S., Carbon Deposit Formation from Thermal Stressing of Petroleum Fuels. *American Chemical Society, Division of Fuel Chemistry*, 2004.

[2] Andresen, J. M., Strohm, J. J., Sun, L., and Song, C., Relationship between the Formation of Aromatic Compounds and Solid Deposition during Thermal Degradation of Jet Fuels in the Pyrolytic Regime. *Energy & Fuels*, vol. 15, no. 3, pp. 714-723, 2001.

[3] Aviation fuels technical review. Chevron Products Company, 2007.

[4] Balster, W.J. and Jones, E.G., Effects of Temperature on Formation of Insoluble in Aviation Fuels. *Journal of Engineering for Gas Turbines and Power*, Vol. 120, pp. 289-293, April 1998.

[5] Ervin, J. S., Heneghan, S. P., Martel, C. R., and Williams, T. F., Surface Effects on Deposits from Jet Fuels. ASME, vol. 118, pp. 278 – 285, April 1996.

[6] Ghamari, M. and Ratner, A. Combustion characteristics of colloidal droplets of jet fuel and carbon based nanoparticles. *Fuel*, vol. 188, pp. 182 – 189, January 2017.

[7] Gul, O., Rudnick, L. R., and Schobert, H. H., Effect of Reaction Temperature and Fuel Treatments on the Deposit Formation of Jet Fuel. *Energy & Fuels*, vol. 22, pp. 433 – 439, 2008.

[8] Hazlett, R. N., Thermal Oxidation Stability of Aviation Turbine Fuels. 1916 Race Street, Philadelphia, PA, U.S.A. 19103: ASTM International, October 1991.

[9] Heneghan, S. P. and Zabarnick, S., Oxidation of jet fuels and the formation of deposits. *Fuel*, vol. 73, no. 1, pp. 35-43, 1994.

[10] Huang, H., Spadaccini, L. J., and Sobel, D. R., Fuel-Cooled Thermal Management for Advanced Aeroengines. *Journal of Engineering for Gas Turbines and Power*, vol. 126, pp. 284-293, April 2004.

[11] Kendall, D. and Mills, J., 1985, The Influence of JFTOT Operating Parameters on the Assessment of Fuel Thermal Stability. SAE Paper No. 851871.

[12] Liu, X. Y. Generic Mechanism of Heterogeneous Nucleation and Molecular Interfacial Effects. *Department of Physics, National University of Singapore*, July 2001.

[13] Omega Thermocouple Technical Report. Online 2016, http://www.omega.com/prodinfo/thermocouples.html (accessed October 21, 2016).

[14] Rawson, P. AMRL Evaluation of the JP-8+100 Jet Fuel Thermal Stability Additive. DSTO Aeronautical and Maritime Research Laboratory. April 2001.

[15] Spadaccini, L. J. and Huang H., On-Line Fuel Deoxygenation for Coke Suppression. *Journal of Engineering for Gas Turbines and Power*, vol. 125, pp. 686-692, July 2003.

[16] Spadaccini, L. J., Sobel, D. R., and Huang, H., Deposit Formation and Mitigation in Aircraft Fuels. *Journal of Engineering for Gas Turbines and Power*, vol. 123, pp. 741-746, October 2001.

[17] Stepka, F. S., Considerations of Turbine Cooling Systems for Mach 3 Flight. *Lewis Research Center, National Aeronautics and Space Administration*, April 1968.

[18] Watkinson A. P. and D. I. Wilson, Chemical Reaction Fouling: A Review. *Experimental Thermal and Fluid Science*, vol. 14, pp. 361-374, 1997.